

# Measuring neutron star tidal deformability with Advanced LIGO: a Bayesian analysis of neutron star - black hole binary observations

Prayush Kumar,<sup>1</sup> Michael Pürer,<sup>2</sup> and Harald P. Pfeiffer<sup>1,3,2</sup>

<sup>1</sup>Canadian Institute for Theoretical Astrophysics, 60 St. George Street, University of Toronto, Toronto, ON M5S 3H8, Canada\*

<sup>2</sup>Albert Einstein Institute, Am Mühlenberg, Golm, Germany

<sup>3</sup>Canadian Institute for Advanced Research, 180 Dundas St. West, Toronto, ON M5G 1Z8, Canada

(Dated: July 29, 2016)

The pioneering discovery of gravitational waves (GW) by Advanced LIGO has ushered us into an era of observational GW astrophysics. Compact binaries remain the primary target sources for GW observation, of which neutron star - black hole (NSBH) binaries form an important subset. GWs from NSBH sources carry signatures of (a) the star's tidal distortion by the companion black hole (BH) during inspiral, and (b) its potential tidal disruption near merger. In this paper, we present a Bayesian study of the measurability of neutron star (NS) tidal deformability  $\Lambda_{\text{NS}} \propto (R/M)_{\text{NS}}^5$  from GW observation(s) of disruptive NSBH coalescences, taking into account the crucial effect of BH spins. First, we find that if BHBH templates are used to estimate source parameters for an NSBH signal, a significant bias is introduced in the inference if the signal-to-noise ratio (SNR) is greater than  $\simeq 30$ . Second, for (loud) signals with  $\text{SNR} \gtrsim 23$  we can bound  $\Lambda_{\text{NS}}$  by a factor of two. Finally, we study the improvement in our measurement of  $\Lambda_{\text{NS}}$  from multiple observations. Using an approximately astrophysical population, we find that (i) the median measured  $\Lambda_{\text{NS}}$  catches up to within 10% of the true value in approximately 20 observations; (ii) in the same number of observations, the associated 90% confidence intervals shrink to  $\pm 50\%$  of the true value. We find these results encouraging, and recommend that an effort to measure  $\Lambda_{\text{NS}}$  be taken within the LIGO-Virgo Collaboration once we begin to detect NSBH coalescences.

## I. INTRODUCTION

The Advanced LIGO (aLIGO) observatories completed their first observing run “O1” early-2016, operating at a factor of 3 – 4 higher gravitational-wave (GW) strain sensitivity than their first-generation counterparts [1]. During O1, they made the first terrestrial observation of gravitational waves [2]. Emitted by a pair of coalescing black holes, these waves have heralded an era of observational GW astrophysics as they traveled through Earth. Towards the end of this decade, we expect aLIGO to reach its design sensitivity. In addition to the US-based efforts, we also expect the French-Italian detector Advanced Virgo [3, 4], Japanese detctor KAGRA [5, 6], and LIGO-India [7] to begin observing at comparable sensitivities within a few years. With a global network of sensitive GW observatories, we can expect GW astronomy to face significant developments over the coming years.

Coalescing compact binaries of stellar-mass black holes (BH) and/or neutron stars (NS) are the primary targets for the second generation GW detectors [8–19]. A binary system of black holes was recently observed by aLIGO [2]. Previously, stellar-mass black holes had only been observed by inference in mixed binaries with stellar companion (through electromagnetic observations of the companion) [20–22]. Neutron stars, on the other hand, have had numerous sightings. Thousands of electromagnetically emitting neutron stars, or pulsars, have been documented [23], in varied situations: as radio pul-

sars [23, 24], in binary systems with a stellar companion [23–26], and in neutron star binaries [23, 24, 27–29]. Mixed binaries of black holes and neutron stars, is an astrophysically interesting class of systems [16, 17, 30, 31], that has not yet been detected. We expect to observe  $\mathcal{O}(10)$  mixed binaries per year with aLIGO [32].

NSBH binaries are of interest for multiple reasons. For instance, they have been long associated with (as possible progenitors of) short Gamma-ray Bursts (SGRBs) [33–41]. Depending on their equation of state (EoS), NSs can get disrupted by the tidal field of their companion BHs. Once disrupted, most of the NS material falls into the hole over an  $\mathcal{O}(1\text{ms})$  time-scale, with the rest partly getting ejected as unbound material and partly forming an accretion disk around the BH. This short lived ( $0.1 - 1\text{s}$ ) disk-BH system is hypothesized to drive SGRBs through the production of relativistic jets [39, 40, 42–45]. However, whether or not such a system forms depends also on the nature of the BH. Massive BHs (with  $m_{\text{BH}} \gtrsim 10M_{\odot}$ ), as well as BHs with large retrograde spins, tend to swallow the NS whole without forming a disk [46]. On the other hand, low-mass BHs with  $m_{\text{BH}} \in [3M_{\odot}, 7M_{\odot}]$ , can disrupt their companion NSs much before merger, forming long-sustained disks that are required to sustain SGRBs [43, 47–49]. A coincident detection of both GWs and gamma-rays from an NSBH merger, will provide us with a unique opportunity to confirm this hypothesized link between NSBH mergers and GRBs [50].

Another question that NSBH mergers can help answer is ‘what is the nature of matter at nuclear densities’, i.e. ‘what is the EoS of NS material’? This is what we will focus on in this paper. During the course of early inspiral, the tidal field of the BH produces a deformation

\* prkumar@cita.utoronto.ca

in its companion NS. The quadrupolar moment of the star associated with this deformation also depends on its material properties, through an EoS-dependent tidal deformability parameter  $\Lambda_{\text{NS}}$ . This induced quadrupolar moment changes over the orbital time-scale, resulting in the emission of GWs in *coherence* with the orbital waves. These waves draw more energy from the orbit and increase the inspiral rate (as compared to an equivalent BBH) [51]. Closer to merger, the strong tidal field of the BH can disrupt the NS. The quadrupolar moment of the disrupted binary system falls monotonically over a millisecond time-scale [42, 43, 52–54]. This penultimate stage also depends strongly on the internal structure and energy transport mechanism of the NS [].

Gravitational waves emitted by coalescing NSBH binaries carry subtle hints of the NS EoS from inspiral through to merger. During early inspiral, the tidal dephasing is relatively weak and appears as a 5<sup>th</sup> Post-Newtonian (PN) order effect [55]. Closer to merger, a disruptive fate of the NS can result in a strong suppression of GW emission above a cut-off frequency [54]. Some past studies of tidal measurements with NSBH binaries have used PN inspiral-only waveforms [56]. In doing so, however, (i) they ignore the merger signal which could contain significant information for NSBHs, and (ii) the errors due to unknown vacuum terms in PN waveforms could dominate over the tidal terms themselves [57, 58]. Some other studies that account for merger effects via the use of complete numerical simulations [46], are limited in the binary parameter space they sample. Others, that do the same through the use of phenomenological waveform models [53, 59] use the Fisher matrix to estimate  $\Lambda_{\text{NS}}$  measurement errors. Fisher matrix estimates are known to be unreliable at realistic signal-to-noise ratios (SNR) [60], such as those as we might expect in the upcoming observing runs of GW detectors [32].

In this paper we study the measurability of neutron star's tidal deformability from realistic binaries of *low*-mass BHs and NSs by aLIGO. We also probe how tidal effects affect the estimation of other binary parameters for the same class of systems. This study improves upon previous work in the following ways. First, we include tidal effects during inspiral and merger in a consistent way, by using the waveform model of Lackey et al. [53] (abbreviated henceforth to “LEA+”). Second, we include the effect of black hole spin on tidal GW signals, in addition to the effect of BH mass, NS's deformability, and the SNR. Third, we perform a complete Bayesian analysis, instead of using the Fisher matrix approximation. Fourth, we explore how our measurement errors decrease as we gain information from multiple (realistic) events.

We first probe the effect of ignoring tidal effects in parameter estimation on the recovery of non-tidal binary parameters, such as component masses and spins. This is the case of current and planned aLIGO efforts. To do so, we first use the LEA+ model to generate a set of realistic signals; and then use non-tidal (BBH) waveform filters to

estimate the underlying binary masses and spins with a Markov-chain Monte Carlo. We find that, for individual events, ignoring tidal effects will affect mass-estimation only marginally; only for very loud signals (SNRs  $\gtrsim 30$ ) will the systematic biases be large enough to exceed the underlying statistical uncertainty. Furthermore, detection searches can ignore tidal effects without loss of sensitivity.

Second, we study the ability of aLIGO to constrain neutron star tidal deformability with a single observation of NSBH merger. For this, we use the same setup for signal waveforms as before, but replace the filter template model with one that includes tidal effects from inspiral through to merger (i.e. LEA+) [53]. For most binaries with BH masses outside of the mass-gap and/or realistic signal-to-noise ratios (SNR), we find it difficult to put better than a factor of 2 bound on  $\Lambda_{\text{NS}}$  with a single observation. As we can see from Fig. 8, it is only at SNRs  $\rho \gtrsim 20 - 30$  (under otherwise favorable circumstances) that we are able to bring this down to a  $\pm 75\%$  bound on  $\Lambda_{\text{NS}}$ . For signals louder than  $\rho = 30$ , we can constrain  $\Lambda_{\text{NS}}$  to a much more meaningful degree (within  $\pm 50\%$  of its true value). While this is discouraging at first, we turn to ask: what if we combine information from a population of low-SNR observations?

The EoS of matter at nuclear densities is believed to be universal among all neutron stars. The Tolman-Oppenheimer-Volkoff equation would then predict that NS properties satisfy a universal relationship between  $\Lambda_{\text{NS}}$  and  $m_{\text{NS}}$ . As the final part of this paper, we combine information from multiple observations of realistic NSBH systems and perform a fully-Bayesian analysis of how our estimation of  $\Lambda_{\text{NS}}$  changes as we accumulate detections. This is similar to an earlier study [61] aimed at binary neutron stars. We restrict ourselves to a population of NSs with masses clustered very tightly around  $1.35M_{\odot}$  (with a negligible variance), and negligible spins. We sample different nuclear EoSs by sampling entire populations fixing different values for the NS tidal deformability. For all populations, we take source locations to be uniformly distributed in spatial volume, and source orientations to be uniform on a 2-sphere. To summarize, we find the following: (a) Our best estimate for  $\Lambda_{\text{NS}}$  improves much faster than our statistical uncertainties. Within 10 – 20 detections, the median measured value of  $\Lambda_{\text{NS}}$  lies within 10% of the actual value. (b) Measurement uncertainties for  $\Lambda_{\text{NS}}$ , on the other hand, depend on  $\Lambda_{\text{NS}}$  itself. We find that for hard equations of state (with  $\Lambda_{\text{NS}} \geq 1000$ ), 10 – 20 observations are sufficient to constrain  $\Lambda_{\text{NS}}$  within  $\pm 50\%$ . For softer equations of state, the same level of certainty would require substantially more (25 – 40) observations. (c) Further, if the astrophysical “mass-gap” is real, we find that 20 – 50% additional observations would be required to attain the same measurement accuracy as above. And, (d) putting tighter constraints on the  $\Lambda_{\text{NS}}$  of a population would require 50+ NSBH observations, in any scenario. All of the above is possible within a few years of design aLIGO

201 operation [62].

202 In this paper, we restrict our parameter space to span  
 203 mass-ratios  $q := m_{\text{BH}}/m_{\text{NS}} \in [2, 5]$ , BH spin (aligned  
 204 with orbit)  $\chi_{\text{BH}} \in [-0.5, +0.75]$ , and dimensionless NS  
 205 tidal deformability  $\Lambda_{\text{NS}} := G \left( \frac{c^2}{Gm_{\text{NS}}} \right)^5 \lambda \in [500, 2000]$ .  
 206 The mass of NS for signals (and not templates) is fixed  
 207 to  $1.35M_{\odot}$  throughout [63]. Similarly, their spin is taken  
 208 to be negligible [64]. Signal strength is sampled over a  
 209 range of SNR  $\rho \in [10, 70]$ . Further, we note that our  
 210 results are applicable for the design sensitivity LIGO in-  
 211 struments (2018 – 19). We also note that the parameter  
 212 space probed is somewhat restricted by the domain of  
 213 applicability of the LEA+ model which we use as filters.  
 214 Finally, the accuracy of our quantitative results depends  
 215 on the reliability of the same waveform model, which is  
 216 the only one available of its kind in current literature. A  
 217 more recent work [65], improves on the GW amplitude  
 218 model, which however needs to be augmented with a com-  
 219 patible phase model. However, we expect the combined  
 220 effect of modeling errors to not change our broad qual-  
 221 itative conclusions, which are based on vague statistical  
 222 trends with large errors themselves.

223 The remainder of the paper is organized as follows.  
 224 Sec. II discusses data analysis techniques and resources  
 225 used in this paper, such as the waveform model, and  
 226 parameter estimation algorithm. Sec. III discusses the  
 227 consequences of ignoring tidal effects in parameter es-  
 228 timation waveform models. Sec. IV discusses the mea-  
 229 surability for the leading order tidal parameter  $\Lambda_{\text{NS}}$  at  
 230 plausible SNR values. Sec. V discusses the improvement  
 231 in our measurement of  $\Lambda_{\text{NS}}$  with successive (multiple)  
 232 observations of NSBH mergers. Finally, in Sec. VI we  
 233 summarize our results and discuss future prospects with  
 234 Advanced LIGO.

251 with NS spin  $\chi_{\text{NS}} = 0$  identically. Here,  $\tilde{h}_{\text{BBH}}$  is an  
 252 underlying BBH waveform model. In the original LEA  
 253 model, this was taken to be the SEOBNRv1 model [66]  
 254 of the Effective-one-body (EOB) family [67]. The factor  
 255  $A(\cdot)$  adjusts the amplitude of the BBH model to match  
 256 that of an NSBH merger of otherwise identical parame-  
 257 ters, with NS-matter effects parametrized by  $\Lambda_{\text{NS}}$ . Dur-  
 258 ing early inspiral this term is set to unity, but is a sen-  
 259 sitive function of  $\Lambda_{\text{NS}}$  close to merger. The term with  
 260  $\Delta\Phi$  corrects the waveform phasing. During inspiral,  $\Delta\Phi$   
 261 is set to the PN tidal phasing corrections, at the leading  
 262 and next-to-leading orders [55]. Close to merger, addi-  
 263 tional phenomenological terms are needed. Both  $A$  and  
 264  $\Delta\Phi$  are calibrated to all 134 available NR simulations.

265 In this paper we use LEA for our signal and tem-  
 266 plate modeling, but switch the underlying BBH model  
 267 to SEOBNRv2 (and refer to it as enhanced-LEA or  
 268 “LEA+”) [68]. We use the reduced-order frequency-  
 269 domain version of SEOBNRv2, which has the additional  
 270 benefit of reducing computational cost [69]. We expect  
 271 this enhancement from LEA → LEA+ to make our conclu-  
 272 sions more robust because: (a) the SEOBNRv2 model is  
 273 more accurate [70, 71], and (b) the differences between  
 274 the two EOB models are caused by the inaccuracies of  
 275 SEOBNRv1 during the *inspiral* phase, many orbits be-  
 276 fore merger [70]. Since LEA only augments inspiral phas-  
 277 ing with PN tidal terms, our change in the underlying  
 278 BBH model does not change LEA’s construction, and  
 279 increases the overall model accuracy during inspiral. Fi-  
 280 nally, we note that we approximate the full GW signal  
 281 with its dominant  $l = |m| = 2$  modes, that are modeled  
 282 by LEA+.

## B. Bayesian methods

283 The process of measuring systematic and statistical  
 284 measurement errors involves simulating many artificial  
 285 GW signals, and inferring source binary parameters from  
 286 them using Bayesian statistics. We start with generating  
 287 a signal waveform, using the model LEA+, and injecting  
 288 it in zero noise to obtain a stretch of data  $d_n$ . Source bi-  
 289 nary parameters  $\vec{\Theta} := \vec{\theta} \cup \{\Lambda_{\text{NS}}\}$  are reconstructed from  
 290 this injected signal. Using Bayes’ theorem, their joint  
 291 inferred probability distribution of  $\vec{\Theta}$  can be written as

$$292 p(\vec{\Theta}|d_n, K) = \frac{p(d_n|\vec{\Theta}, K) p(\vec{\Theta}|K)}{p(d_n|K)}. \quad (2)$$

293 Here,  $p(\vec{\Theta}|K)$  is the a-priori probability of binary par-  
 294 ameters taking particular values. Throughout this paper, we  
 295 impose a prior uniform on individual component masses,  
 296 BH spin, and NS’s tidal deformability. In addition, we  
 297 restrict mass-ratios to  $q \geq 2$ , as LEA+ is not calibrated  
 298 for  $1 \leq q \leq 2$ .  $p(d_n|\vec{\Theta}, K)$  is the likelihood of obtaining  
 299 the given stretch of data  $d_n$  if we assume that a signal  
 300 parameterized by  $\vec{\Theta}$  is buried in it, and is given by

$$301 p(d_n|\vec{\Theta}, K) \equiv \mathcal{L}(\vec{\Theta}) = \mathcal{N} \exp[-\langle d_n - h | d_n - h \rangle], \quad (3)$$

## II. TECHNIQUES

### A. Waveform Models

302 Lackey et al. (LEA) [53] developed a complete inspiral-  
 303 merger waveform model for disrupting NSBHs. Theirs  
 304 is a frequency-domain phenomenological model that in-  
 305 cludes the effect of BH and NS masses and spins  
 306  $\{m_{\text{BH}}, \chi_{\text{BH}}, m_{\text{NS}}\} \equiv \vec{\theta}$  and NS tidal deformability  $\Lambda_{\text{NS}}$ .  
 307 It was calibrated to a suite of 134 numerical relativity  
 308 (NR) simulations of NSs inspiraling into spinning BHs.  
 309 The parameter space these simulations span, which we  
 310 assume to be the domain of validity for the LEA model,  
 311 includes NS masses  $1.2M_{\odot} \leq m_{\text{NS}} \leq 1.45M_{\odot}$ , mass-  
 312 ratios  $2 \leq q \leq 5$ , and BH spins  $-0.5 \leq \chi_{\text{BH}} \leq +0.75$ .  
 313 They also sample a total of 21 two-parameter nuclear  
 314 EoSs to cover the spectrum of NS deformability. The  
 315 GW strain  $\tilde{h}(f)$  per the LEA model can be written as  
 316

$$317 \tilde{h}_{\text{NSBH}}(f, \vec{\theta}, \Lambda_{\text{NS}}) = \tilde{h}_{\text{BBH}}(f, \vec{\theta}) A(f, \vec{\theta}, \Lambda_{\text{NS}}) e^{i\Delta\Phi(f, \vec{\theta}, \Lambda_{\text{NS}})}, \\ 318 \quad (1)$$

where  $h \equiv h(\vec{\Theta})$  is a filter template with parameters<sup>342</sup>  $\vec{\Theta}$ , and  $\langle \cdot | \cdot \rangle$  is a suitably defined detector-noise weighted<sup>343</sup> inner-product<sup>1</sup>. [MP: INSERT A LINE ABOUT AP<sup>344</sup> PROXIMATING  $\mathcal{L} \approx e^{\rho^2/2}$ <sup>345</sup>] The denominator in Eq. 2 is<sup>346</sup> the a-priori probability of finding the particular signal in<sup>347</sup>  $d_n$  and we assume that each injected signal is as likely<sup>348</sup> as any other. Having constructed the probability dis-<sup>349</sup> tribution function  $p(\vec{\Theta}|d_n, K)$ , extracting the measured<sup>349</sup> probability distribution for a single parameter (say  $\alpha$ )<sup>350</sup> involves integrating<sup>351</sup>

$$p(\alpha|d_n, K) = \int d\vec{\Theta}_\alpha p(\vec{\Theta}|d_n, K), \quad (5)$$

where  $\vec{\Theta}_\alpha$  is the set of remaining parameters, i.e.  $\vec{\Theta}_\alpha := \vec{\Theta} - \{\alpha\}$ .

We use an ensemble sampler Markov-chain Monte-Carlo algorithm based on the `emcee` package [72], to sample the probability distribution  $p(\vec{\Theta}|d_n, K)$ . We start with 100 independent walkers, each of which is allowed to collect 100,000 samples. One simplification we make to mitigate computational cost is to set the frequency sampling interval to  $\Delta f = 0.4$  Hz, which we find to be sufficient for robust likelihoods calculations [73]. Once more than 10,000 independent samples have been collected, we integrate Eq. 5 to obtain marginalized probability distributions for the NS tidal deformability parameter:  $p(\Lambda_{\text{NS}}|d_n, K)$ . The median value of this distribution is our *measured* value for  $\Lambda_{\text{NS}}$ , and the 90% confidence intervals associated with the distribution serve as statistical error-bars.

### III. HOW IS PE AFFECTED IF WE IGNORE NS MATTER EFFECTS?

Past and future GW search and source characterization efforts with Advanced LIGO have used (or plan to) BH-BH waveform templates for NS-BH mergers, ignoring NS tidal effects on the emitted GWs. In this section we present a fully Bayesian analysis of the effects of this assumption on the recovery of NSBH masses and spins from their GW signals.

We construct NSBH waveforms using the LEA+ model. We inject these into zero noise and run MCMC on the injections using BBH templates (LEA+ with tidal terms set to zero). We perform this analysis for a variety of mass ratios  $q \in \{2, 3, 4, 5\}$ , i.e.

$m_{\text{BH}} \in \{2.7M_\odot, 4.05M_\odot, 5.4M_\odot, 6.75M_\odot\}$ , and BH spins  $\chi_{\text{BH}} \in \{-0.5, 0, +0.5, +0.75\}$ . We always use  $m_{\text{NS}} = 1.35M_\odot$  and  $\chi_{\text{NS}} = 0$ , but explore  $\Lambda_{\text{NS}} \in \{500, 800, 1000, 1500, 2000\}$ . The signal strength is varied from  $\rho = 20 \rightarrow 70$ . Our choice of this SNR range is motivated by previous studies which suggest that signatures of NS tidal effects become observable only at relatively large SNRs [53], and is validated by results that follow. At design sensitivity, if we expect 10 – 300 NSBH detections a year [62], and if BH masses are uniformly likely up to  $\sim 35M_\odot$  [2], we would expect to detect 0.3 – 7 disruptive NSBH mergers a year with  $\rho \geq 20$ , 0.07 – 2 a year with  $\rho \geq 30$ , and 0.04 – 1 a year with  $\rho \geq 70$ . For our priors, we choose uniform distribution for both component masses as well as for black hole spins, i.e.  $m_{\text{BH}} \in [2, 20]M_\odot$ ,  $m_{\text{NS}} \in [1, 3]M_\odot$  and  $-0.5 \leq \chi_{\text{BH}} \leq +0.75$ . **FIXME**

As an illustration, in Fig. 1 we show the probability distribution for binary mass ratio  $\eta$  recovered from a GW injection with intrinsic parameters:  $m_{\text{NS}} = 1.35M_\odot$ ,  $\chi_{\text{NS}} = 0$ ,  $m_{\text{BH}} = 5.4M_\odot$ ,  $\chi_{\text{BH}} = +0.5$  and  $\Lambda_{\text{NS}} = 2000$ , and SNRs ranging from  $\rho = 20$  (left panel) to  $\rho = 50$  (right panel). In each panel, the *true* value of  $\eta$  is marked by a dashed green line, and its measured (median) value by a dashed red line. The effect of ignoring tidal corrections in templates manifests as a systematic shift of the measured  $\eta$  value away from its true value. The associated *systematic* bias/error is given by the difference between measured and true  $\eta$  values. Darker shading of the probability distribution marks the 90% confidence interval for  $\eta$ , whose width is a direct measure of the *statistical* measurement uncertainty/error. We clearly see that even when the signal is moderately loud, with  $\rho = 20$ , statistical errors dominate over systematics completely for  $\eta$ . As we turn up the SNR further, we find that the two error sources become comparable at  $\rho \sim 30$ , and systematic errors dominate finally when  $\rho \simeq 50$ .

Next, to get a better understanding of how *precisely* we measure NSBH binary parameters given BBH waveforms, we show the 90% confidence intervals associated with NSBH mass and spin measurements in Fig. 2. The three panels, corresponding to  $\mathcal{M}_c$  (top),  $\eta$  (middle), and  $\chi_{\text{BH}}$  (bottom), show the width of these confidence intervals as a function of BH mass/spin (within each sub-panel), and NS properties, i.e.  $\Lambda_{\text{NS}}$  (downwards in each column)<sup>2</sup>. From the left-most column, we find that: (i) at  $\rho = 20$ ,  $\mathcal{M}_c$  is already measured remarkably well – to a precision of 0.16% of its true value, and (ii) so is  $\chi_{\text{BH}}$ . (iii) Mass ratio  $\eta$  is determined more loosely, with  $\gtrsim 25\%$  uncertainty. If the signal is even louder ( $\rho \geq 30$ ), all three measurements gain further precision, with  $\eta$  errors shrinking down to single-digit percents of its true

<sup>1</sup> The inner product  $\langle \cdot | \cdot \rangle$  is defined as

$$\langle a|b \rangle \equiv 4 \text{Re} \left[ \int_0^\infty \frac{\tilde{a}(f)\tilde{b}(f)^*}{S_n(|f|)} df \right], \quad (4)$$

where  $\tilde{a}(f)$  is the Fourier transform of the finite time series  $a(t)$ , and  $S_n(|f|)$  is the one-sided amplitude spectrum of detector noise.

<sup>2</sup> We restrict NS mass to  $1.35M_\odot$  and its spin to zero. Varying its tidal deformability  $\Lambda_{\text{NS}}$  does not change the measurement uncertainties for non-tidal binary parameters, as is evident from comparing the two rows in each panel of Fig. 2.

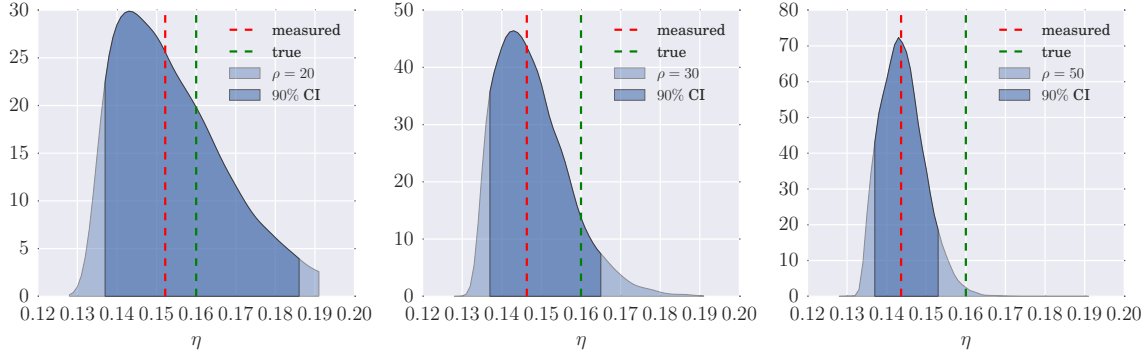


FIG. 1. We show here probability distributions for mass ratio  $\eta$  as measured for the same injection at different SNRs. The intrinsic parameters of the source are:  $q = m_{\text{BH}}/m_{\text{NS}} = 5.4M_{\odot}/1.35M_{\odot} = 4$ ,  $\chi_{\text{BH}} = +0.5$ , and  $\Lambda_{\text{NS}} = 2000$ ; and the signal is injected at SNRs  $\rho = \{20, 30, 50\}$  (left to right). The templates ignore tidal effects. In each panel: the dashed red line marks the median *measured* value  $\eta^{\text{Median}}$ , while the dashed green line shows the true value  $\eta^{\text{Injected}}$ . The difference between the true and measured values is the systematic bias introduced by ignoring tidal effects in templates. The darker shading shows the recovered 90% confidence interval for  $\eta$ ,  $(\Delta\eta)^{90\%}$ , which is a direct measure of our statistical uncertainty on  $\eta$ . Comparing systematic and statistical errors, we find that: at  $\rho = 20$ ,  $\eta$  measurement is dominated by statistical errors; at  $\rho = 30$ , the two become comparable; and for louder signals ( $\rho \simeq 50$ ), the systematic errors dominate.

value. However, we remind ourselves that there are physical effects that have not been incorporated in our (BBH) search templates which we use here to decipher NSBH signals. Therefore, we cannot know the *accuracy* of our parameter measurements unless we know how large the systematic biases due to an incomplete template model are. To quantify this, we find it useful to define  $\mathbf{r}$ , the ratio of the systematic biases induced by unmodeled tidal effects in templates, to the statistical uncertainties associated with the measurement itself. If  $\mathbf{r} \gtrsim 1$ , including the effect of NS's tidal distortion (during inspiral) and possible disruption (close to merger) would be imperative to obtain *accurate* estimates of source masses and spins from observed GW signals.

We first calculate the ratio of errors  $\mathbf{r}$  associated with chirp mass measurements and show it in Fig. 3.  $\mathcal{M}_c$  is the mass combination that affects at leading order the GW strain emitted by compact binaries as they spiral in, and is therefore determined the most precisely. From the left-most column of the figure, we find that even at  $\rho = 30$ , the systematic bias in  $\mathcal{M}_c$  measurement is much smaller than its statistical uncertainty. For signals with  $\rho \leq 30$ , therefore, we are justified in using BBH templates to estimate binary chirp mass from NSBH signals. For louder and less realistic SNRs (say  $\rho = 50$ ), we find that  $\mathbf{r}$  can become comparable to unity if additionally: (i) the BH has a prograde spin  $\chi_{\text{BH}} \gtrsim 0.4$ , and (ii) the NS's true deformability is large enough, s.t.  $\Lambda_{\text{NS}} \gtrsim 1000$ . It is only at SNRs as high as  $\rho \simeq 70$  that the systematic biases for  $\mathcal{M}_c$  exceed the underlying statistical uncertainty to become the dominant source of errors. We conclude that only for  $\rho \gtrsim 50 - 70$  do we need to include in our templates terms that capture the effect of neutron star's structural dynamics on emitted GWs. For lower SNRs, improvements in template model will be washed out by

the statistical measurement uncertainty for  $\mathcal{M}_c$ . Lastly, we note that  $\mathbf{r}$  is always positive for  $\mathcal{M}_c$ , suggesting that it is always over-estimated. This is understandable since the tidal deformation of NSs close to merger reduces the GW signal power at high frequencies, which would make the resulting signal resemble a BBH signal of higher mass (and therefore lower merger frequency).

Next, in Fig. 4, we show the ratio of measurement errors  $\mathbf{r}$  for the symmetric mass-ratio  $\eta$ . We immediately observe that the measured (median)  $\eta$  is always lowered below its true value due to the lack of  $\Lambda_{\text{NS}}$ -dependent terms in the filter template model. This bias, similar to the  $\mathcal{M}_c$  bias, reduces the merger frequency for BBH templates, in order to better match the relatively quiet merger and ringdown of NSBHs. At  $\rho = 30$ , the systematic bias in  $\eta$  measurement stays mostly around 10–50% of its statistical measurement uncertainty. For the sole case of a very deformable NS with  $\Lambda_{\text{NS}} = 2000$ , can the effect of missing tidal pieces in the template model become comparable to that of noise (which is usually more restrictive on measurements). For a still stronger signal with  $\rho = 50$ , we find that when the following conditions are fulfilled, the measurement of  $\eta$  is unreliable due to template biases: (a) BH mass  $m_{\text{BH}} \leq 5M_{\odot}$ , (b) BH spin  $\chi_{\text{BH}} \gtrsim +0.4$ , and (c)  $\Lambda_{\text{NS}} \gtrsim 1500$ . Even under more moderate restrictions on BH and NS parameters, we find that  $\rho = 50$  is loud enough to motivate the use of tidal-modeled templates. This observation is further strengthened if we divert our attention to the third column in Fig. 4 that presents the case for even higher SNRs ( $\rho = 70$ ).

Moving on from mass to spin parameters, we now consider the measurement of spin angular momentum of the BH  $\chi_{\text{BH}}$ . The ratio of the systematic bias introduced into and the statistical uncertainty associated with  $\chi_{\text{BH}}$

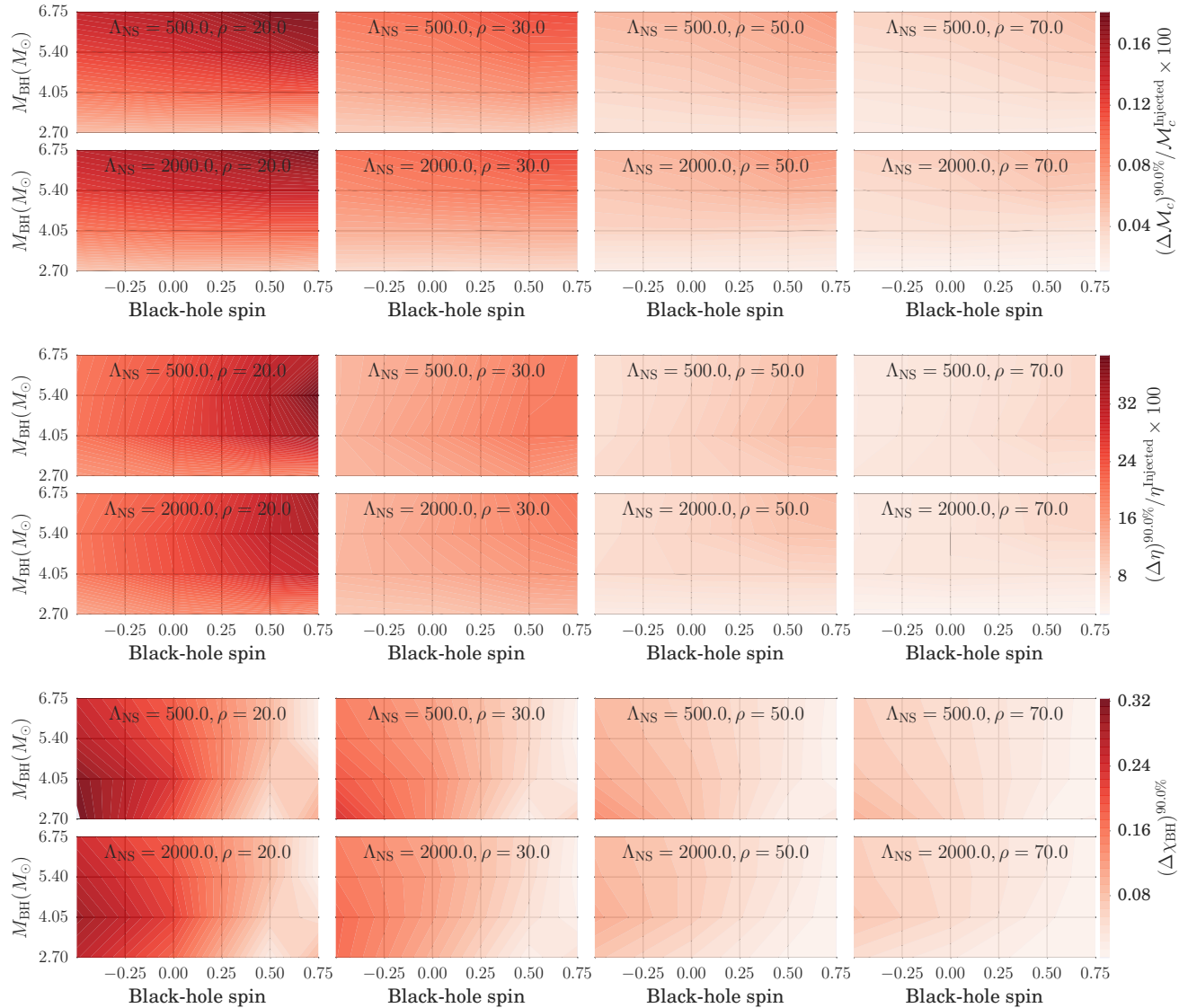


FIG. 2. We show here the statistical uncertainty of our measurement of the dimensionless mass ratio  $\eta$  (at 90% confidence), over the NSBH parameter space. Individual panels show the same as a function of BH mass and spin. Across each row, we see the effect of increasing signal strength (i.e. SNR) with the NS's tidal deformability  $\Lambda_{\text{NS}}$  fixed. Down each column, we see the effect of increasing  $\Lambda_{\text{NS}}$ , at fixed SNR.

measurement is shown in Fig. 5. The presentation of in-<sup>478</sup>  
formation in this figure is identical to that in Fig. 3 and 4.<sup>479</sup>  
A diverging colormap is used because both extremes of<sup>480</sup>  
the colorbar range point to large systematic biases, while<sup>481</sup>  
its zero (or small) value lies in the middle. For the lowest<sup>482</sup>  
considered SNR  $\rho = 30$ ,  $\chi_{\text{BH}}$  bias is negligible, being be-<sup>483</sup>  
low 50% of its statistical measurement uncertainty. For<sup>484</sup>  
the most deformable NS structure *and* with a low-mass<sup>485</sup>  
BH, the statistical bias in  $\chi_{\text{BH}}$  does become an impor-<sup>486</sup>  
tant error. This is furthered at higher SNR, consider-<sup>487</sup>  
ing  $\rho = 50$  next (middle column of Fig. 5). We find that for<sup>488</sup>  
low-mass BHs (with masses below  $4.5M_{\odot}$ ), the system-<sup>489</sup>  
atic measurement bias for BH spin exceeds its statistical<sup>490</sup>  
uncertainty to become the dominant source of error. Not<sup>491</sup>

surprisingly, the systematic bias at both spin extremes pushes towards milder spins, since the prior excludes any more extreme spins than  $[-0.75, +0.75]$  and that pushes the bulk of the posterior inwards. However as the signal's  $\Lambda_{\text{NS}}$  is increased from  $500 \rightarrow 2000$ , low-mass BH-NS binaries with large spins on the BH show very large systematic biases in spin values, that become larger than the statistical uncertainty for  $\rho \geq 30$  and reach up to  $4 \times$  the same quantity as  $\rho \rightarrow 70$ .

Summarizing these results, we find that irrespective of system parameters, below a signal-to-noise ratio of 30, our measurements of mass and spin parameters of astrophysical BHNS binaries will remain limited by the intrinsic uncertainty due to instrument noise, and do not

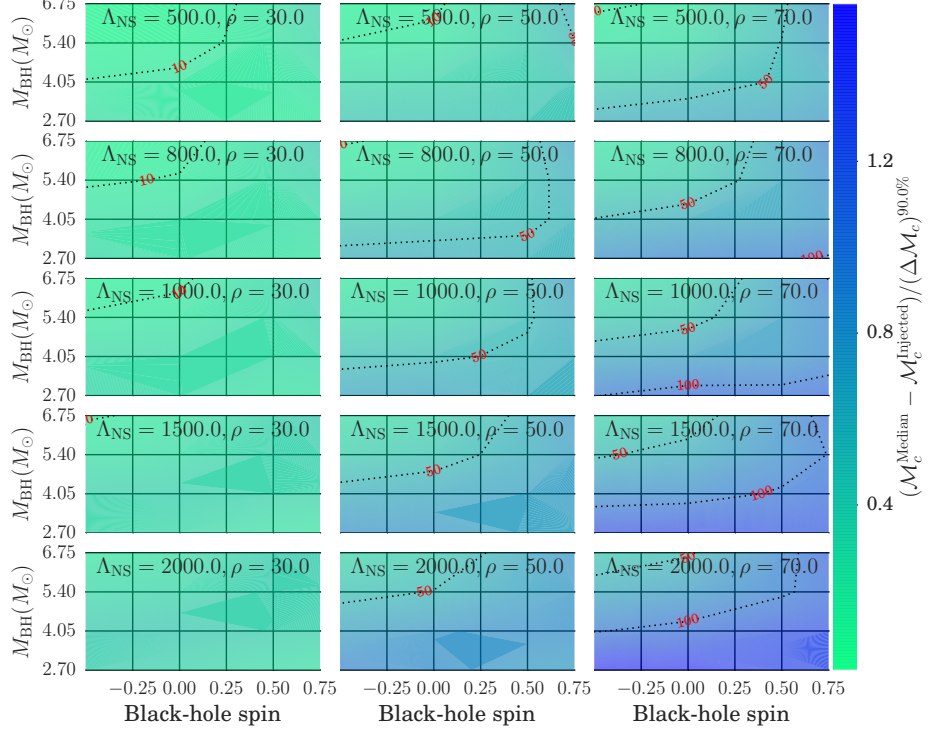


FIG. 3. We show here the ratio of systematic and statistical measurement uncertainties for the binary chirp mass over the NSBH parameter space. Each panel shows the same as a function of BH mass and spin. Across each row, we can see the effect of increasing the signal strength (i.e. SNR) with the NS's deformability fixed. Down each column, we can see the effect of the increasing NS's tidal deformability at fixed SNR. We also show dashed contours for where the ratio equals 10% (labelled “-1”) or 100% (labelled “0”). Generally, these two sources of uncertainty are different and for BBHs, the statistical errors dominate systematic ones [71]. We find that for BHNS binaries, its not much different until we get to high SNRs  $\rho \gtrsim 70$  for which if the BH is spinning rapidly enough, the measurement uncertainty for  $\mathcal{M}_c$  could become dominated by the exclusion of tidal effects in filtering templates.

depend on whether we include tidal effects in template models. However, when the signal-to-noise ratio exceeds 30 the systematic bias in binary mass and spin measurements become comparable to and exceed the uncertainty due to noise. Of the different parameters considered, we find that the measurement of  $\eta$  degrades worst (in a relative-error sense) amongst all other parameters of BHNS binaries, due to the use of BH-BH waveforms in deciphering an NSBH signal.

its GW SNR  $\gtrsim 30$ . The first two conditions both enhance the tidal distortion of the star and increase the number of orbits the system goes through at small separation, where the differences between NSBH and BHB signals are maximal. The first three also reduce the onset frequency of NS’s disruption, allowing for it to happen earlier in the orbit. We expect that these conditions are also the ones which would maximize the likelihood of *measuring* tidal effects in NSBH signals. In this section, we turn the question around and ask: under similarly favorable circumstances, can we gain insights about the internal structure of neutron stars from GW observations.

#### IV. WHAT DO WE GAIN BY USING TEMPLATES THAT INCLUDE NS MATTER EFFECTS?

In the previous section, we showed that the effect of NS’s deformation due to its companion BH’s quadrupolar tidal field becomes discernible in the GW spectrum only when the following hold: (a) the BH has a sufficiently small mass, (b) BH spin is positive aligned, i.e.  $\chi_{\text{BH}} \gtrsim +0.4$ , (c) the NS is not very compact, with  $\Lambda_{\text{NS}} \gtrsim 1000$ , and (d) the source is close enough such that

We begin by calculating the accuracy with which we measure  $\Lambda_{\text{NS}}$  from *single* GW observations. We sample the same set of disruptive NSBH systems as in the previous section, i.e. those with  $q = \{2, 3, 4, 5\}$ ,  $\chi_{\text{BH}} = \{-0.5, 0, +0.5, +0.75\}$ , and  $\Lambda_{\text{NS}} = \{500, 800, 1000, 1500, 2000\}$ ; fixing the NS mass  $m_{\text{NS}} = 1.35M_{\odot}$  and  $\chi_{\text{NS}} = 0$ . For each unique combination of these parameters, we generate separate zero-noise injections at SNRs  $\rho = \{20, 30, 50, 70\}$ , using the LEA+ model. We perform full Bayesian analyses on each of

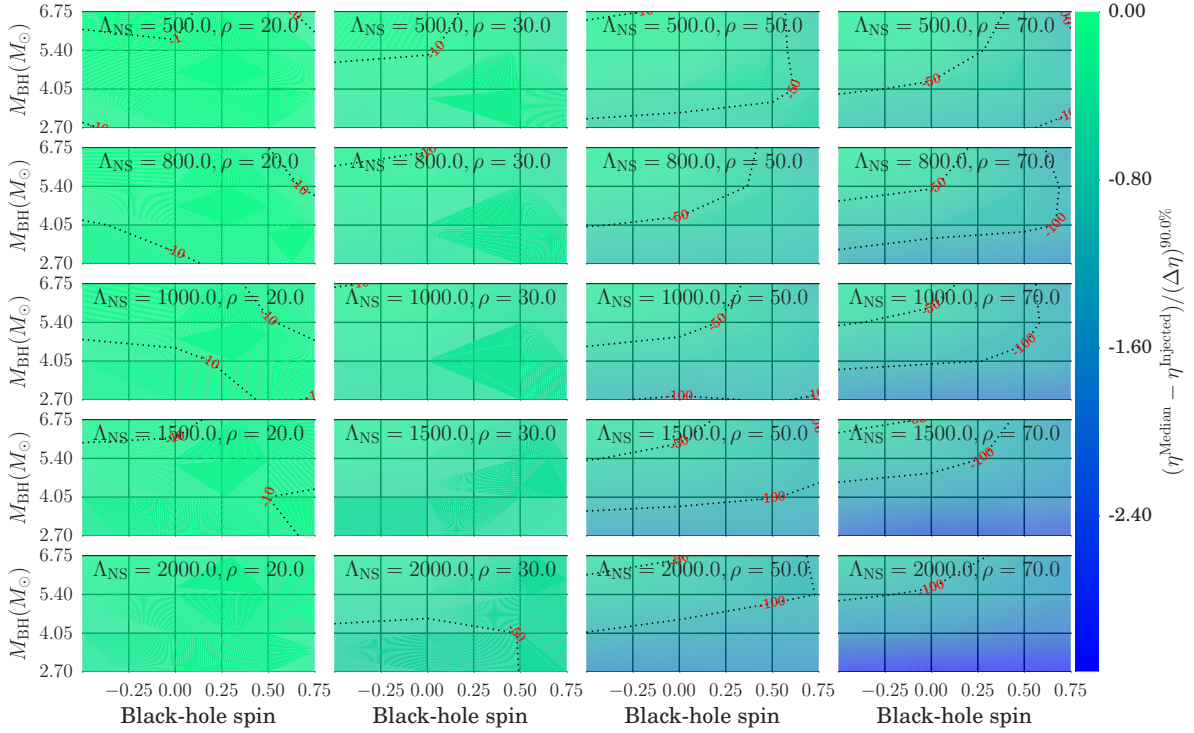


FIG. 4. This figure is similar to Fig. 3 with the difference that the quantity in question here is the symmetric mass-ratio  $\eta$ . We find that for fairly loud GW signals, with  $\rho \simeq 50$ , not including the effects of NS's tidal deformation on GW emission can become the dominant source of error for astrophysical searches with Advanced LIGO. However, for quieter signals with  $\rho \leq 30$ , it will have minimal effects on the measurement of  $\eta$ . We remind the reader that the SNRs here are all single detector values.

these injections using LEA+ templates, and obtain probabilistic estimates for source binary parameters using GW information alone (including the NS tidal deformability parameter  $\Lambda_{\text{NS}}$ ). Our priors on component masses and spins remain as in the previous section, while  $\Lambda_{\text{NS}}$  is sampled uniformly from  $[0, 4000]$ .

As an illustration, we show the recovered probability distribution for  $\Lambda_{\text{NS}}$  for three specific configurations in Fig. 6. We fix  $q = m_1/m_2 = 5.4M_\odot/1.35M_\odot = 4$ , with  $\chi_{\text{BH}} = +0.5$ , while varying  $\Lambda_{\text{NS}}$  over  $\{1000, 1500, 2000\}$  between the three panels. The SNR is fixed at  $\rho = 50$ . The true value of  $\Lambda_{\text{NS}}$  is given by the green (dashed) vertical line, while the median recovered value is marked by a red (dashed) line. The darker shaded region marks the 90% confidence interval on  $\Lambda_{\text{NS}}$ . One thing to note in this figure is that the measurement uncertainty on  $\Lambda_{\text{NS}}$ , i.e. the full width of its 90% confidence interval, grows slower than  $\Lambda_{\text{NS}}$  as  $\Lambda_{\text{NS}}$  is turned up (while the fractional uncertainty

$$\delta\Lambda_{\text{NS}}^{90\%} := (\Delta\Lambda_{\text{NS}})^{90\%}/\Lambda_{\text{NS}} \quad (6)$$

parameters, as manifested in their recovered joint probability distributions. In the middle row, we show the same between  $\Lambda_{\text{NS}}$  and non-tidal parameters, i.e. chirp mass (left panel), mass ratio  $\eta$  (middle panel), and BH spin  $\chi_{\text{BH}}$  (right panel). The same is shown in the row below, with the difference that the SNR has been turned up to  $\rho = 50$ , which brings out the intrinsic ambiguity contours more clearly. We find that the measurement of  $\Lambda_{\text{NS}}$  is weakly degenerate with other parameters, and at realistic SNRs it would improve by a few tens of percent if we knew non-tidal parameters to better accuracy. The predominant factor that would enhance the measurement accuracy for  $\Lambda_{\text{NS}}$  is the signal strength, and only when  $\rho \gtrsim 50$  do we expect  $\Lambda_{\text{NS}}$  measurement to be limited by its degeneracy with non-tidal parameters at a factor of few level, as was reported by Ref. [53].

In Fig. 8 we show the main results of this section. In each panel, as a function of black hole mass and spin, we show the measured 90% confidence intervals for  $\Lambda_{\text{NS}}$ , i.e.  $(\Delta\Lambda_{\text{NS}})^{90\%}$ . These correspond to the full width of the dark shaded region in the illustrative figure, Fig. 6. The effect of signal strength, i.e. SNR, can be seen as we go from left to right in each row. The effect of NS's tidal deformability  $\Lambda_{\text{NS}}$  on its own measurability can be seen by comparing panels within each column. The NS becomes more deformable as

decreases with increasing  $\Lambda_{\text{NS}}$ ). Next, in Fig. 7 we show the correlation of mass, spin, and tidal parameter measurements. We keep the binary parameters as in Fig. 6, with  $\Lambda_{\text{NS}} = 2000$ , and  $\rho = 30$  (instead of 50). In the top panel, we show the correlation between non-tidal pa-

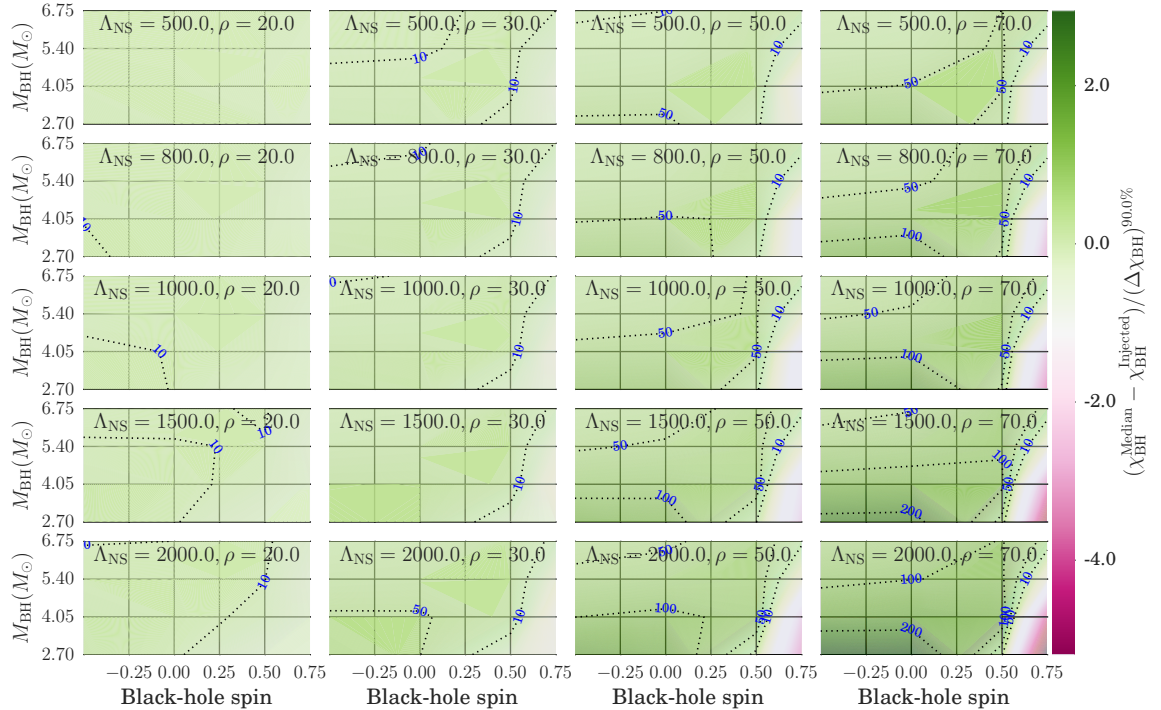


FIG. 5. This figure shows the ratio of the systematic and statistical measurement errors for BH spins, with other attributed identical to Fig. 3, and 4. Similar to the case of mass parameters, we find that below  $\rho \approx 30$ , ignoring tidal effects in templates introduces minor systematic effects, which remain subdominant to the statistical measurement uncertainties.

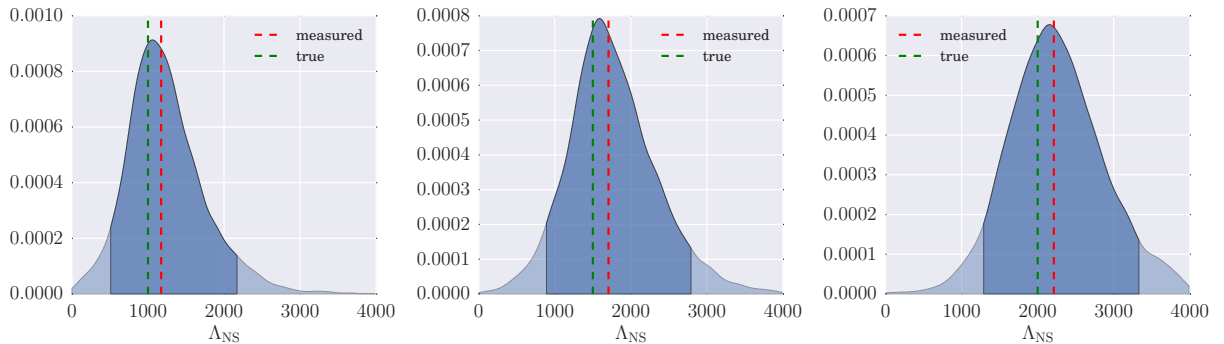


FIG. 6. We illustrate here probability distributions recovered for the NS tidal deformability parameter  $\Lambda_{\text{NS}}$  from three GW injections, with parameters:  $q = m_{\text{BH}}/m_{\text{NS}} = 5.4M_{\odot}/1.35M_{\odot} = 4$ ,  $\chi_{\text{BH}} = +0.5$ , and  $\Lambda_{\text{NS}} = \{1000, 1500, 2000\}$  from left to right. The injection SNR is fixed at  $\rho = 50$ . The templates include tidal effects, with a prior  $0 \leq \Lambda_{\text{NS}} \leq 4000$ . In each panel- the dashed red line marks the median *measured* value for  $\Lambda_{\text{NS}}$ , and the dashed green line marks its *true* value. The darker shading shows the 90% confidence interval, whose width  $(\Delta\Lambda_{\text{NS}})^{90\%}$  is a direct measure of our statistical uncertainty. By comparing the measurement uncertainty for these three injections, we see that  $(\Delta\Lambda_{\text{NS}})^{90\%}$  grows very slowly with  $\Lambda_{\text{NS}}$ . Therefore, the fractional measurement error -  $(\Delta\Lambda_{\text{NS}})^{90\%}/\Lambda_{\text{NS}}$  - decreases monotonically as  $\Lambda_{\text{NS}}$  increases (with signal strength fixed).

we go from top to bottom. In addition, contours of  $\delta\Lambda_{\text{NS}}^{90\%} = \{50\%, 75\%, 100\%, 150\%, 200\%\}$  are also shown in all panels. A clear pattern emerges in the left-most column, which corresponds to  $\rho = 20$ . We find that at this signal strength, our measurement of  $\Lambda_{\text{NS}}$  is dominated by the width of our prior on  $\Lambda_{\text{NS}}$ . In other words, our

measured confidence interval is restricted by the allowed range of  $\Lambda_{\text{NS}}$ . Increasing the signal strength to  $\rho = 30$  gives somewhat similar results, as can be seen from the second-from-left column of the figure. We do, however, find more encouraging results for high BH spins, in which

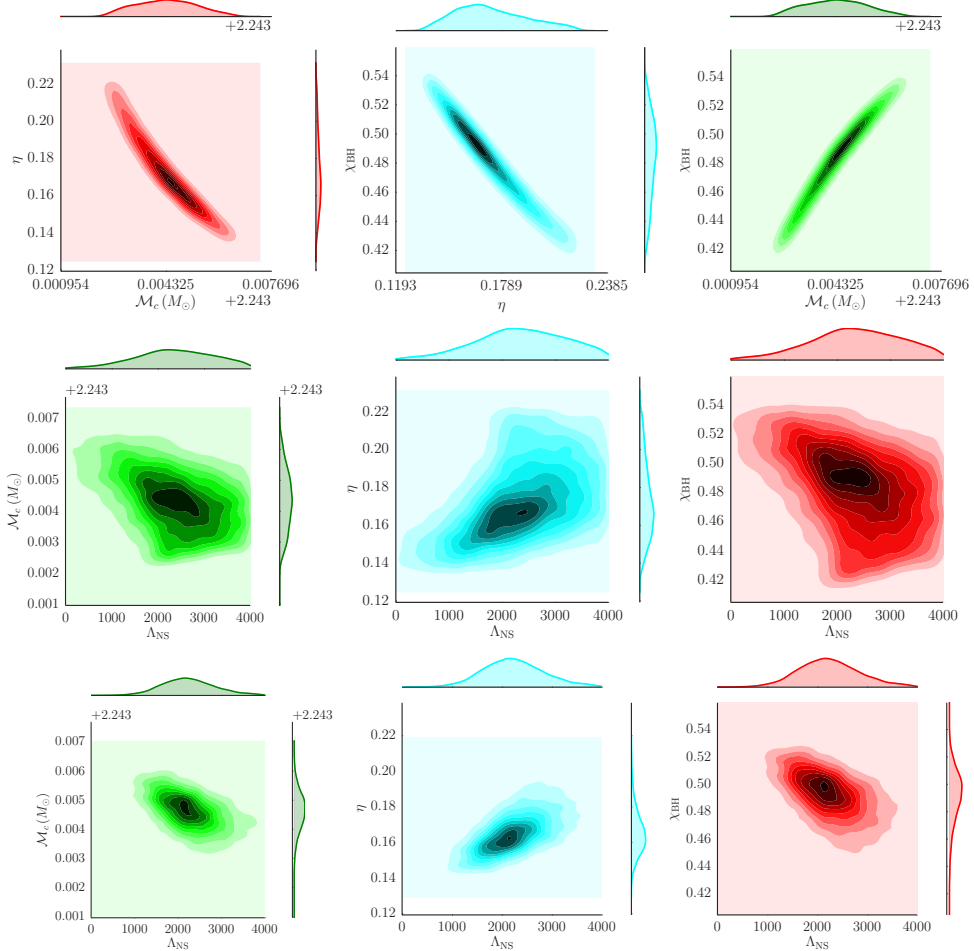


FIG. 7. We illustrate here two-dimensional joint probability distributions, as recovered for the intrinsic parameters of a binary with  $q = m_{\text{BH}}/m_{\text{NS}} = 5.4M_{\odot}/1.35M_{\odot} = 4$ ,  $\chi_{\text{BH}} = +0.5$ ,  $\Lambda_{\text{NS}} = 2000$ , and  $\rho = 30$  (same as in Fig. 6). The top row shows the same for combinations of non-tidal parameters, i.e. binary masses and spins, while the middle row shows combinations of  $\Lambda_{\text{NS}}$  with non-tidal parameters. The bottom row is similar to the middle, with the only difference being that the SNR has been turned up to  $\rho = 50$ .

case we can put  $\pm 100\%$  to  $\pm 75\%$  bounds on  $\Lambda_{\text{NS}}$ <sup>3</sup>. In addition to large BH spins, this level of precision will also require rather deformable neutron stars. At higher SNRs,  $\rho \gtrsim 50$ , we can put stronger constraints on  $\Lambda_{\text{NS}}$ . With a single observation of a  $q = 4$  binary with  $\chi_{\text{BH}} \geq 0.6$  and  $\rho = 50$ <sup>4</sup>, we would be able to estimate  $\Lambda_{\text{NS}}$  to within  $\pm 40\%$  of its true value (which is equivalent to measuring the ratio of its radius to mass with an uncertainty of about  $\pm 10\%$ ).

Amongst other source parameters, BH mass and spin play a dominant role. A smaller BH with a larger spin always allows for a more precise measurement on  $\Lambda_{\text{NS}}$ . Usually we can see this in the bottom right corner of each

panel in Fig. 8, which corresponds to low-mass BHs with large spins, and is simultaneously the region of smallest measurement errors on  $\Lambda_{\text{NS}}$ . The actual deformability of the NS also plays an important role on its own measurability. For e.g., when  $\Lambda_{\text{NS}} \leq 1000$ , it is fairly difficult to meaningfully constrain  $\Lambda_{\text{NS}}$  without requiring the source to be close ( $\approx 100\text{Mpc}$ ) with a GW SNR  $\rho \gtrsim 50$ . Quantifying this further, in Fig. 9 we show the minimum signal strength required to attain a certain level of confidence in our  $\Lambda_{\text{NS}}$  measurement, as a function of BH properties. The NS is allowed the most favorable (hardest) EoS considered, with  $\Lambda_{\text{NS}}^{\text{true}} = 2000$ . We first note that, even with the most favorable BH and NS properties, achieving a  $\pm 50\%$  measurement certainty on  $\Lambda_{\text{NS}}$  will require a GW SNR  $\rho \gtrsim 30$ . If we additionally restrict BH masses to lie outside of the so-called astrophysical mass-gap [74–77], we will simultaneously need to restrict BH spins to  $\chi_{\text{BH}} \gtrsim +0.5$  to obtain the same measurement confidence at the same source location.

<sup>3</sup> The symmetric error-bars of  $\pm X\%$  correspond to  $\delta\Lambda_{\text{NS}}^{90\%} = 2X\%$

<sup>4</sup> For an optimally oriented source with  $q = 4$ ,  $m_{\text{NS}} = 1.35M_{\odot}$ ,  $\chi_{\text{BH}} = 0.6$ , an SNR of  $\rho = 50$  corresponds to a luminosity distance of  $\approx 113\text{Mpc}$ .

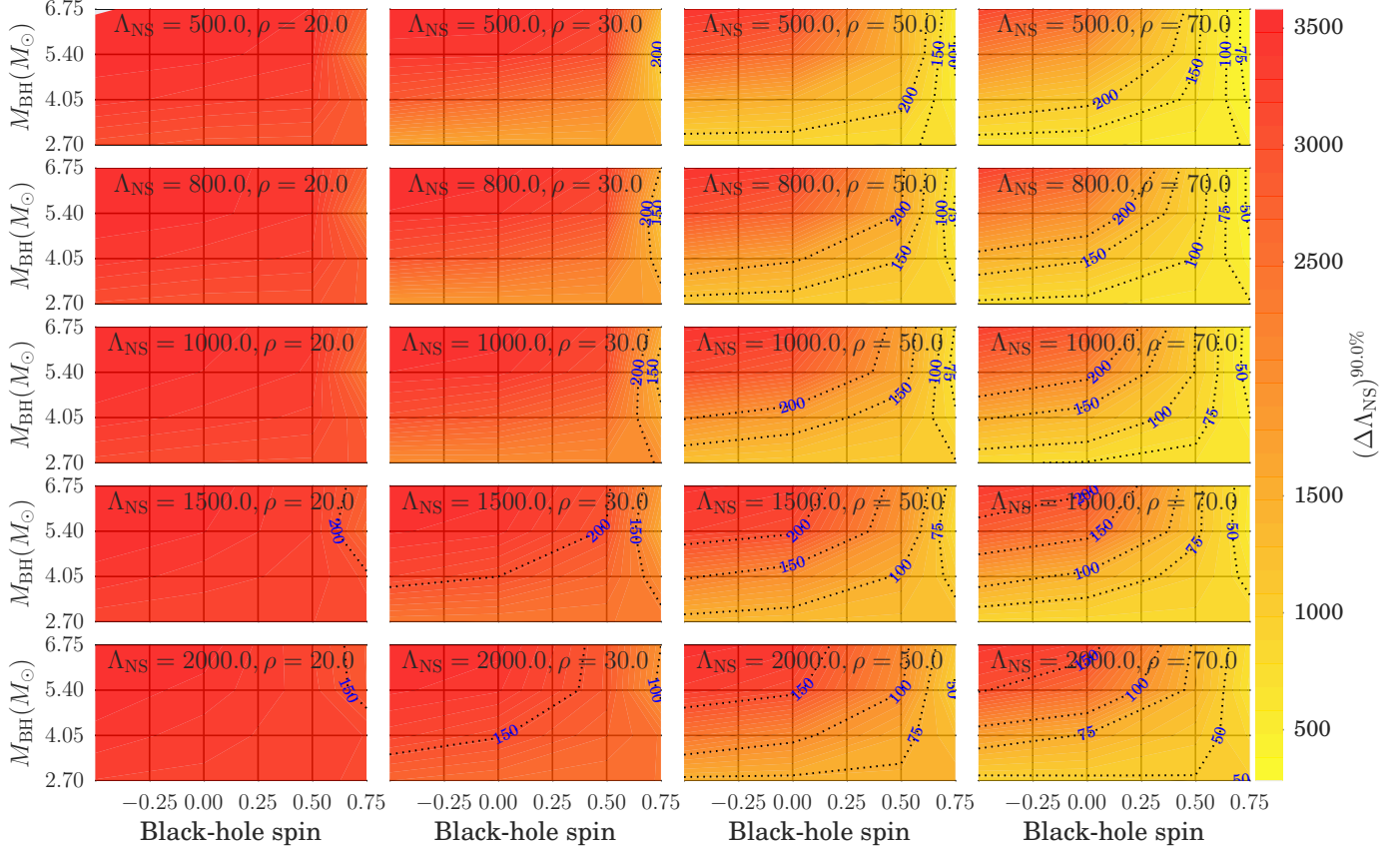


FIG. 8. Here we show the statistical uncertainty in the measurement of  $\Lambda_{\text{NS}}$ , as a percentage of the injected/true value. In each panel, the same is shown as a function of the BH mass and spin, keeping  $\Lambda_{\text{NS}}$  and injection's SNR  $\rho$  fixed (noted in the panel). Each row contains panels with the same value of  $\Lambda_{\text{NS}}$ , with  $\rho$  increasing from left to right. Each column contains panels with the same value of  $\rho$ , with  $\Lambda_{\text{NS}}$  increasing from top to bottom. Contours demarcate regions where we can constrain the  $\Lambda_{\text{NS}}$  parameter well (within a factor of two of the injected value). We note that, as expected, the measurement accuracy for  $\Lambda_{\text{NS}}$  improves with (i) increasing SNR, (ii) decreasing BH mass, (iii) increasing BH spin, and (iv) increasing  $\Lambda_{\text{NS}}$ , i.e. the tidal deformability of the neutron star.

In summary, with a single moderately loud ( $\rho \lesssim 30$ )<sub>642</sub> GW signal from a disruptive BHNS coalescence, we can<sub>643</sub> constrain the NS compactness parameter  $\Lambda_{\text{NS}}$  within<sub>644</sub>  $\pm 100\%$  of its true value. To measure better with one<sub>645</sub> observation, we will need a more fine-tuned source, with<sub>646</sub>  $\rho \geq 30$  and high BH spins, or  $\rho \geq 50$ . Finally, we note<sub>647</sub> that these results are *conservative*, and BHs with spins<sub>648</sub>  $\chi_{\text{BH}} > 0.75$  will prove to be even more favorable labora<sub>649</sub> tories for  $\Lambda_{\text{NS}}$  measurement. However, we are presently<sub>650</sub> unable to explore this case in quantitative detail due to<sub>651</sub> waveform model restrictions [53], which will restrict our<sub>652</sub> analyses of actual GW signals as well.<sub>653</sub>

information about the internal structure of neutron stars that will be accessible to Advanced LIGO at its design sensitivity. We expect all neutron stars to share the same equation of state, and hence the same  $\Lambda_{\text{NS}}(m_{\text{NS}})$ . In addition, we know that the mass distribution of (most) NSs that have not been spun up to millisecond periods (which are what we focus on in this paper, by approximating  $\chi_{\text{NS}} \approx 0$ ) is narrowly peaked around  $\sim 1.35 M_{\odot}$  [78]. Therefore, information from multiple NSBH observations can be combined to improve our estimation of  $\Lambda_{\text{NS}}$  for the population. This is what we explore in this section, within a fully Bayesian framework.

## 638 V. COMBINING OBSERVATIONS: LOOKING 639 FORWARD WITH ADVANCED LIGO

640 In the previous section, we showed that single observa<sub>641</sub>  
tions of NSBH coalescences at moderate SNRs have little

An intuitive understanding of the problem is gained by considering first multiple *identical* sources at realistic SNRs. Let us consider the case a population of optimally

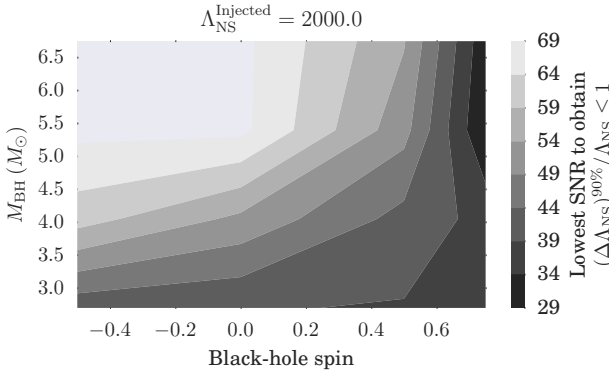


FIG. 9. We show here, as a function of BH mass and spin, the *minimum* signal strength (SNR) required to constrain  $\Lambda_{\text{NS}}$  within an interval of width equal to 100% of its true value, i.e. with  $\pm 50\%$  error-bars. The NS mass is fixed at  $1.35 M_{\odot}$ , spin at zero, and  $\Lambda_{\text{NS}} = 2000$ . We can see that, even in the most conducive circumstances with large aligned  $\chi_{\text{BH}}$  and a comparable mass BH, we can only constrain  $\Lambda_{\text{NS}}$  to better than  $\pm 50\%$  if the SNR is  $\gtrsim 29$ . In the era of design sensitivity LIGO instruments, we expect this to happen approximately once in a year of observation.

oriented binaries<sup>5</sup>, distributed uniformly in spacial volume out to a maximum distance  $D^{\max}$ .  $D^{\max}$  is set by the minimum SNR threshold  $\rho_{\min}$  at which a source is considered detectable<sup>6</sup>. Next, we divide this volume into  $I$  concentric shells, with radii  $D_i$ . If we have a measurement error  $\sigma_0$  for  $\Lambda_{\text{NS}}$ , associated with a source located at  $D = D_0$ , the same error for the same source located within the  $i$ -th shell would be  $\sigma_i = \sigma_0 \frac{D_i}{D_0}$ . Ref. [79] calculated that the combined error  $\sigma$  from  $N$  independent measurements of  $\Lambda_{\text{NS}}$  in such a setting to be

$$\begin{aligned} \frac{1}{\sigma^2} &= \sum_{i=1}^I \frac{N_i}{\sigma_i^2} = \left( \frac{D_0}{\sigma_0} \right)^2 \sum_{i=1}^I \frac{N_i}{D_i^2} \\ &= \left( \frac{D_0}{\sigma_0} \right)^2 \int_0^{D^{\max}} \frac{4\pi D^2 n}{D^2} dD = \left( \frac{D_0}{\sigma_0} \right)^2 \frac{3N}{(D^{\max})^2}, \end{aligned} \quad (7)$$

where  $N_i$  is the number of sources within the  $i$ -th shell (s.t.  $N := \sum N_i$ ), and  $n$  is the number density of sources in volume. The root-mean-square (RMS) averaged measurement error from  $N$  sources is then [79]

$$\sigma_{avg} := \frac{1}{\sqrt{1/\sigma^2}} = \frac{\sigma_0}{D_0} D^{\max} \frac{1}{\sqrt{3N}}, \quad (8)$$

<sup>5</sup> An optimally oriented binary is one which is located directly overhead the detector, with the orbital angular momentum parallel to the line joining the detector to the source. Such a configuration maximizes the observed GW signal strength in the detector.

<sup>6</sup> which we take as  $\rho_{\min} = 10$  throughout.

given a fiducial pair  $(\sigma_0, D_0)$ . It is straightforward to deduce from Eq. 8 that measurement uncertainty scales as  $1/\sqrt{N}$ , and the uncertainty afforded by a single observation with a high SNR  $\rho_c$  can be attained with  $N = \rho_c^2/300$  realistic observations that have  $\rho \geq \rho_{\min}$ . E.g., to get to the level of certainty afforded by a single observation with  $\rho = 70$ , we would need  $49/3 \approx 16-17$  realistic (low SNR) detections.

While we discussed Eq. 8 for a population of optimally oriented sources, it is valid more generally for a population distributed uniformly in *effective* volume<sup>7</sup> [79]. However, it still only applies to sources with identical masses and spins, and we overcome this limitation by performing a fully Bayesian analysis next.

**Astrophysical source population:** Imagine that we have  $N$  stretches of data,  $d_1, d_2, \dots, d_N$ , each containing a single signal emitted by an NSBH binary. Each of these signals can be characterized by the non-tidal source parameters  $\vec{\theta} := \{m_{\text{BH}}, m_{\text{NS}}, \chi_{\text{BH}}, \chi_{\text{NS}}, \vec{\alpha}\}$ , and  $\{\Lambda_{\text{NS}}\}$ , where  $\vec{\alpha}$  contains extrinsic parameters, such as source distance, inclination, and sky location angles. Further, let  $K$  denote all of our collective prior knowledge, except for expectations on binary parameters themselves, which enter the following calculation explicitly. For instance,  $K$  includes our assumption that all NS's in a single population have the same deformability parameter  $\Lambda_{\text{NS}}$ , and its cumulative measurement is therefore possible. The probability distribution for  $\Lambda_{\text{NS}}$ , given  $N$  unique and independent events, is

$$\begin{aligned} p(\Lambda_{\text{NS}} | d_1, d_2, \dots, d_N, K) &= \frac{p(d_1, d_2, \dots, d_N | \Lambda_{\text{NS}}, K) p(\Lambda_{\text{NS}} | K)}{\int p(\Lambda_{\text{NS}} | K) p(d_1, d_2, \dots, d_N | \Lambda_{\text{NS}}, K) d\Lambda_{\text{NS}}}, \quad (9) \\ &= \frac{p(\Lambda_{\text{NS}} | K) \prod_i p(d_i | \Lambda_{\text{NS}}, K)}{\int p(\Lambda_{\text{NS}}) p(d_1, d_2, \dots, d_N | \Lambda_{\text{NS}}, K) d\Lambda_{\text{NS}}}, \quad (10) \\ &= \frac{p(\Lambda_{\text{NS}} | K) \prod_i \left( p(\Lambda_{\text{NS}} | d_i, K) \frac{p(d_i)}{p(\Lambda_{\text{NS}} | K)} \right)}{\int p(\Lambda_{\text{NS}} | K) p(d_1, d_2, \dots, d_N | \Lambda_{\text{NS}}, K) d\Lambda_{\text{NS}}}; \quad (11) \end{aligned}$$

where Eq. 9 and Eq. 11 are application of Bayes' theorem, while Eq. 10 comes from the mutual independence of all events. Assuming in addition that all events are *equally*

<sup>7</sup> *effective* distance  $D_{\text{eff}}$  is a combination of distance to the source, its orientation, and its sky location angles, and has a one-to-one correspondence with SNR for non-precessing systems, for which these angles are constant in time. Effective volume is  $\frac{4\pi}{3} D_{\text{eff}}^3$ .

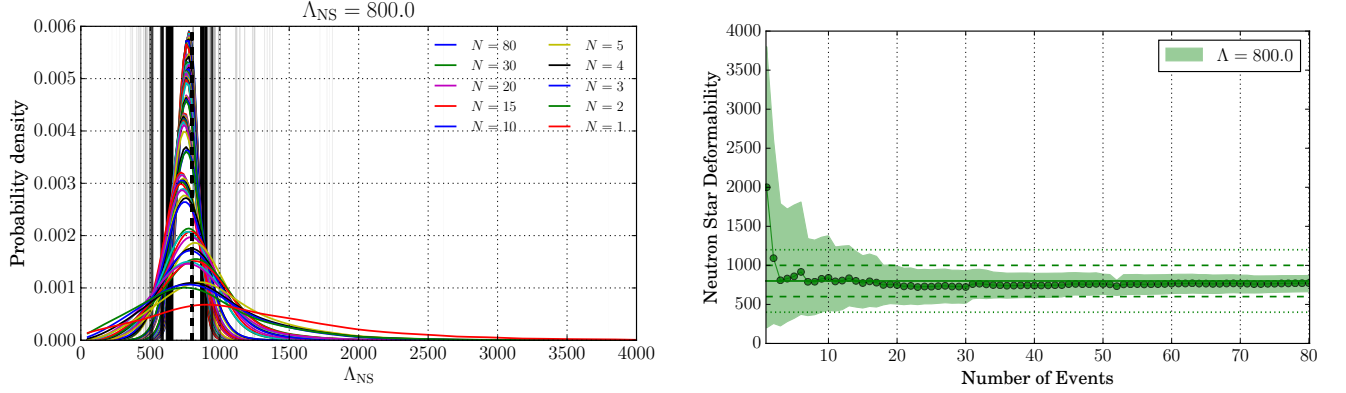


FIG. 10. These panels show the accumulation of information from a population whose  $\Lambda_{\text{NS}} = 800$ . *Left:* Posterior probability distributions for  $\Lambda_{\text{NS}}$  (colored curves), and associated 90% confidence intervals (grey vertical lines), shown for different number of accumulated observations  $N$ . Distributions are normalized to unit area. *Right:* Measured median value of  $\Lambda_{\text{NS}}$  (as solid circles) and the associated 90% confidence intervals (as the vertical extent of filled region), shown as a function of number of observations  $N$ . Solid horizontal line indicates the true value of  $\Lambda_{\text{NS}}$ . Dashed and dotted horizontal lines (a pair for each line-style) demarcate  $\pm 25\%$  and  $\pm 50\%$  error bounds.

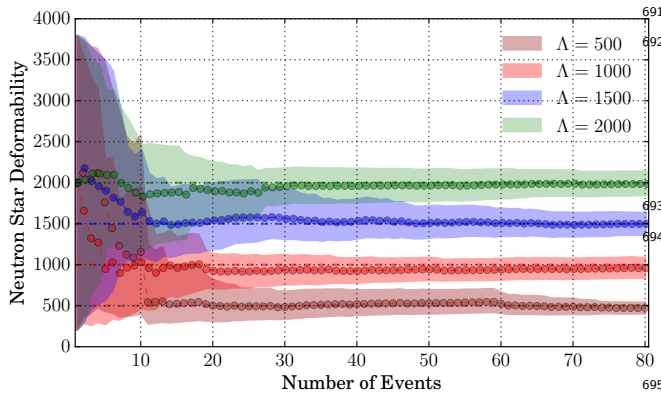


FIG. 11. In this figure, the filled regions show how our measurement of  $\Lambda_{\text{NS}}$  improves as the number of observed events ( $N$ , shown on  $x$ -axis) increases. Each color corresponds to an independent population with its true value of  $\Lambda_{\text{NS}}$  given in the legend. For each population, we show the median measured  $\Lambda_{\text{NS}}$  value (as filled circles), as well as the associated 90% confidence intervals for the measurement (as the vertical extent of the filled region about the median), as functions of  $N$ .

The first two factors in Eq. 13 can be absorbed into a normalization factor  $\mathcal{N}$ , simplifying it to

$$p(\Lambda_{\text{NS}}|d_1, d_2, \dots, d_N; K) = \mathcal{N} \prod_{i=1}^N p(\Lambda_{\text{NS}}|d_i, K). \quad (14)$$

A priori, we assume that no particular value of  $\Lambda_{\text{NS}}$  is preferred over another, and restrict  $\Lambda_{\text{NS}}$  to  $[0, 4000]$ , i.e.

$$p(\Lambda_{\text{NS}}|K) = \frac{1}{4000} \text{Rect}\left(\frac{\Lambda_{\text{NS}} - 2000}{4000}\right). \quad (15)$$

In the second set of terms in Eq. 14 (of the form  $p(\Lambda_{\text{NS}}|d_i, K)$ ), each is the probability distribution for  $\Lambda_{\text{NS}}$  inferred *a posteriori* from the  $i$ -th observation by marginalizing

$$p(\Lambda_{\text{NS}}|d_i, K) = \int p(\vec{\theta}, \Lambda_{\text{NS}}|d_i, K) d\vec{\theta}, \quad (16)$$

where  $p(\vec{\theta}, \Lambda_{\text{NS}}|d_i, K)$  is the inferred joint probability distribution of all source parameters  $\vec{\theta} \cup \{\Lambda_{\text{NS}}\}$  for the  $i$ -th event, as given by Eq. 2. We note that Fig. 6 illustrates  $p(\Lambda_{\text{NS}}|d_i, K)$  for three individual events. By substituting Eq. 15–16 into Eq. 14, we calculate the probability distribution for  $\Lambda_{\text{NS}}$  as measured using  $N$  independent events.

Our goal is to understand the improvement in our measurement of  $\Lambda_{\text{NS}}$  with the number of recorded events. To do so, we simulate a population<sup>8</sup> of  $N$  events, and quantify what we learn from each successive observation

<sup>8</sup> A population here is an ordered set of events, and an event itself is the set of parameters describing one astrophysical NSBH binary.

likely:  $p(d_i) = p(d_j) = p(d)$ , we get

$$\begin{aligned} p(\Lambda_{\text{NS}}|d_1, d_2, \dots, d_N, K) &= p(\Lambda_{\text{NS}}) \left( \frac{p(d)}{p(\Lambda_{\text{NS}})} \right)^N \prod_i p(\Lambda_{\text{NS}}|d_i, K) \\ &= \frac{p(\Lambda_{\text{NS}})}{\int p(\Lambda_{\text{NS}}) p(d_1, d_2, \dots, d_N | \Lambda_{\text{NS}}, K) d\Lambda_{\text{NS}}} \prod_i p(\Lambda_{\text{NS}}|d_i, K), \end{aligned} \quad (13)$$

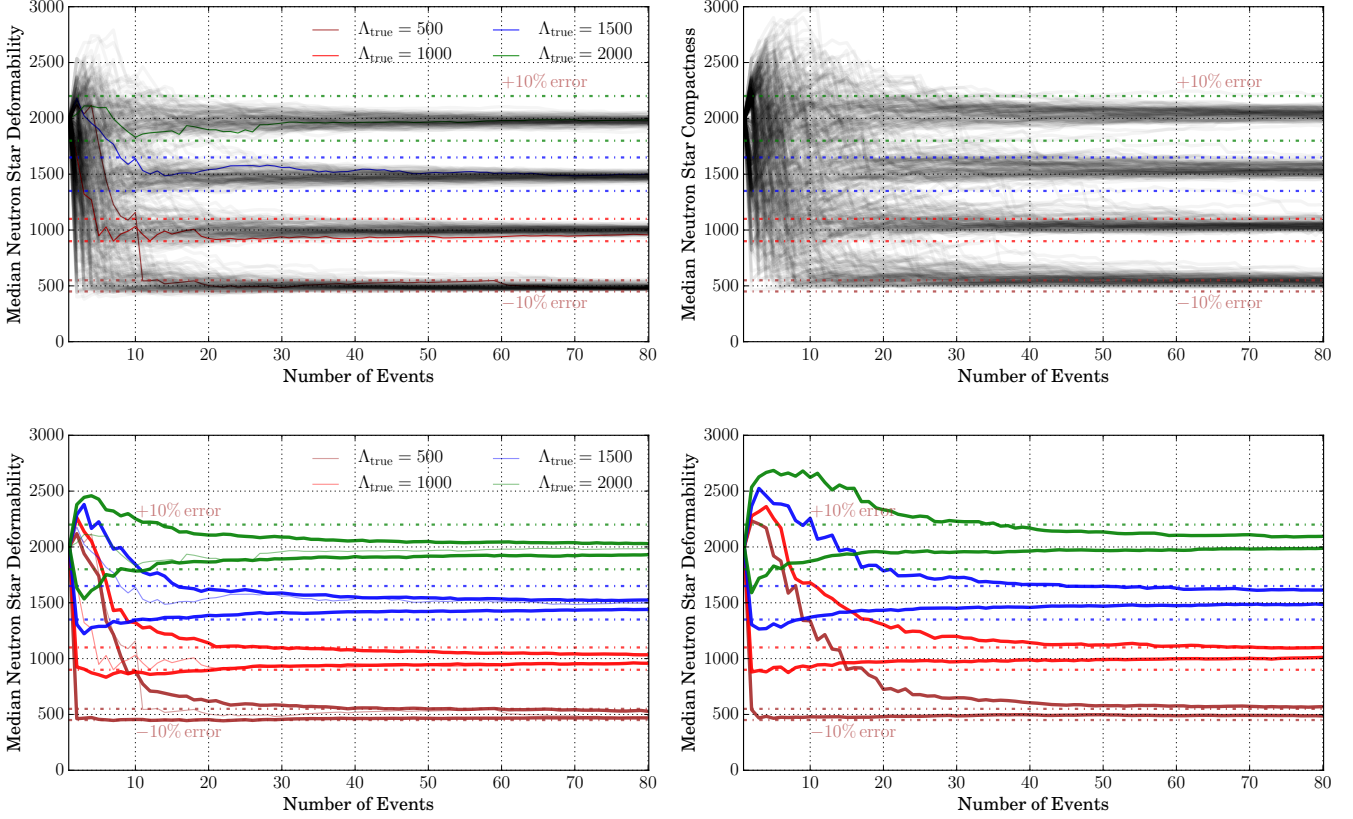


FIG. 12. *Top left:* This figure shows the median value of the recovered probability distribution for  $\Lambda_{\text{NS}}$ , as a function of the number of events in the population  $N$ . There are four ensembles of curves, corresponding to  $\Lambda_{\text{NS}} = \{500, 1000, 1500, 2000\}$ , with a hundred independent population draws within each ensemble. One curve in each ensemble is highlighted in color, representing only that it is the same population as was discussed in Fig. 10–11. In the same color we show  $\pm 10\%$  error-bounds on  $\Lambda_{\text{NS}}$  with horizontal dash-dotted lines. *Bottom left:* Here we show the interval of  $\Lambda_{\text{NS}}$  values within which the median measured  $\Lambda_{\text{NS}}$  lies for 90% of the populations in each ensemble shown in the top left panel. We observe that within 10 – 25 observations, the median of the measured cumulative probability distribution for  $\Lambda_{\text{NS}}$  converges to within 10% of its true value. *Right:* These panels are identical to their counterparts on the left, with the only difference that the BH masses in each population are restricted to lie *outside* the astrophysical mass-gap (i.e. paradigm B). The difference that we observe under this paradigm is that we need more (30+) events to achieve the same (10%) measurement accuracy for populations with  $\Lambda_{\text{NS}} < 1000$ . For more deformable neutron stars, 10 – 25 events would suffice.

710 using Eq. 14. This allows us to quantify how rapidly<sup>727</sup>  
 711 our median estimate for  $\Lambda_{\text{NS}}$  converges to the true value,<sup>728</sup>  
 712 and how rapidly our confidence intervals for the same<sup>729</sup>  
 713 shrink, with increasing  $N$ . Finally, we generate and ana-<sup>730</sup>  
 714 lyze an ensemble of populations in order to average over<sup>731</sup>  
 715 the stochastic process of population generation itself.<sup>732</sup>

716 In order to generate each population, the first step is<sup>733</sup>  
 717 to fix the NS properties: (i) NS mass  $m_{\text{NS}} = 1.35M_{\odot}$ , (ii)<sup>734</sup>  
 718 NS spin  $\chi_{\text{NS}} = 0$  and (iii) NS tidal deformability  $\Lambda_{\text{NS}} =$ <sup>735</sup>  
 719 fixed value chosen from  $\{500, 800, 1000, 1500, 2000\}$ .<sup>736</sup>  
 720 Next, we generate events, by sampling BH mass (uni-<sup>737</sup>  
 721 formly) from  $m_{\text{BH}} \in [3M_{\odot}, 6.75M_{\odot}]$ , BH spin (uni-<sup>738</sup>  
 722 formly) from  $\chi_{\text{BH}} \in [0, 0.75]$ , source location uniformly in  
 723 spatial volume, and its inclination from  $\iota \in [0, \pi]$ . Note<sup>740</sup>  
 724 that we only sample positive aligned BH spins, since bi-<sup>741</sup>  
 725 naries with anti-aligned spins have very little information<sup>742</sup>  
 726 to add at realistic SNRs, as shown in Fig. 8. As noted<sup>743</sup>

previously, we also restrict events to have  $\rho \geq \rho_{\min}$ , where  
 $\rho_{\min} = 10$ . Finally, we repeat the process till we have an  
 ordered set of  $N$  events. Since we want to analyze not  
 just a single realization of an astrophysical population,  
 but an ensemble of them, we make an additional ap-  
 proximation to mitigate computational cost. Complete  
 Bayesian parameter estimation is performed for a set of  
 simulated signals whose parameters are the vertices of a  
 regular hypercubic grid (henceforth “G”) in the space of  
 $\{q\} \times \{\chi_{\text{BH}}\} \times \{\rho\}$ , with each sampled at  $q = \{2, 3, 4, 5\}$ ,  
 $\chi_{\text{BH}} = \{-0.5, 0, 0.5, 0.75\}$ , and  $\rho = \{10, 20, 30, 50, 70\}$ . All events in each population draw are substituted by  
 their respective nearest neighbours on the grid G.

In Fig. 10 we show illustrative results for a single popu-  
 lation with neutron star deformability  $\Lambda_{\text{NS}} = 800$ . In the  
 left panel, each curve shows the probability distributions  
 for  $\Lambda_{\text{NS}}$  as inferred from  $N$  events, with  $N$  ranging from

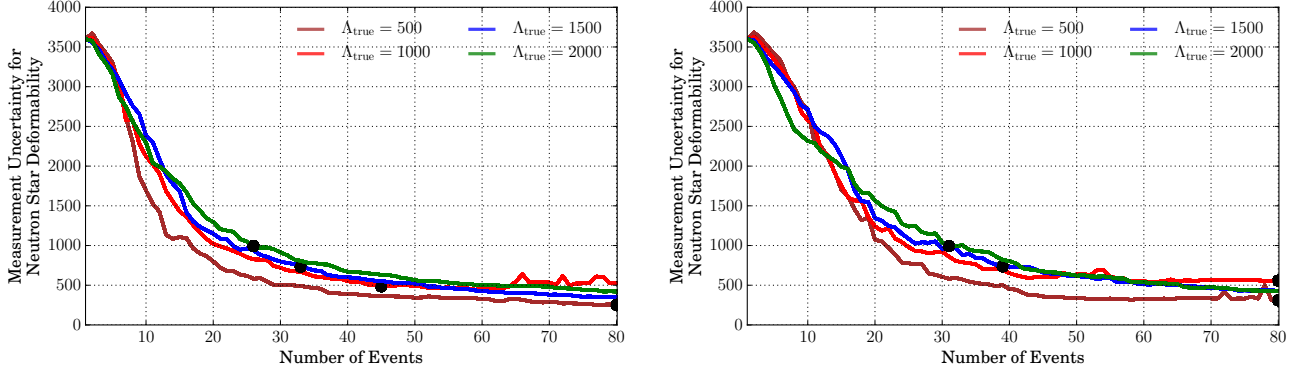


FIG. 13. *Left:* This panel shows the width of  $\Lambda_{\text{NS}}$  interval within which the 90% confidence intervals for  $\Lambda_{\text{NS}}$  lie, for 90% of the populations in each ensemble, as a function of the number of observed events  $N$ . Details of how this is calculated are given in the text. The populations are sampled under paradigm A, which allows BH masses to fall within the astrophysical mass-gap. Each panel corresponds to a unique value of populations'  $\Lambda_{\text{NS}}$ , decreasing from 2000  $\rightarrow$  500 as we go from top to bottom. *Right:* This panel shows populations drawn under paradigm B, which respects the mass-gap. We find that with approximately 25 or so events, we begin to put statistically meaningful constraints on  $\Lambda_{\text{NS}}$ , restricting it to within  $\pm 50\%$  of the true value. We can expect to achieve this with a few years of design aLIGO operation [62]. Further tightening of  $\Lambda_{\text{NS}}$  confidence intervals will require 40+ events.

744 1 – 80. We also mark the 90% confidence intervals as<sup>779</sup>  
 745 associated with each of the probability distribution curves.<sup>780</sup>  
 746 The first few observations do not have enough informa<sup>781</sup>  
 747 tion to bound  $\Lambda_{\text{NS}}$  much more than our prior from Eq. 15<sup>782</sup>  
 748 does. However, the median of these cumulative distribu<sup>783</sup>  
 749 tions appears to track the true value of  $\Lambda_{\text{NS}}$  rapidly. In<sup>784</sup>  
 750 the right panel, we present information derived from the<sup>785</sup>  
 751 left panel. The line-circle curve shows the measured me<sup>786</sup>  
 752 dian from  $N$  observations. The pair of dashed (dotted)<sup>787</sup>  
 753 horizontal lines mark  $\pm 25\%$  ( $\pm 50\%$ ) error bars. At each<sup>788</sup>  
 754  $N$ , the range spanned by the filled region is the 90%<sup>789</sup>  
 755 confidence interval deduced from the same events. This<sup>790</sup>  
 756 figure somewhat quantifies the qualitative deductions we<sup>791</sup>  
 757 made from the left panel. We find that the measured<sup>792</sup>  
 758 median does track the true value quickly, reaching 10%<sup>793</sup>  
 759 accuracy with 10 – 15 observations. With the same in-<sup>794</sup>  
 760 formation, our confidence intervals also shrink to  $\pm 25\%$ .<sup>795</sup>  
 761 In Fig. 11 we show further results from four indepen-<sup>796</sup>  
 762 dent populations for  $\Lambda_{\text{NS}} = \{500, 1000, 1500, 2000\}$ . As<sup>797</sup>  
 763 in the right panel of Fig. 10, the line-circle curves track<sup>798</sup>  
 764 the median measured  $\Lambda_{\text{NS}}$ , while the filled regions show<sup>799</sup>  
 765 the associated 90% confidence intervals. From the figure,<sup>800</sup>  
 766 we observe the following: (i) the shrinkage of confidence<sup>801</sup>  
 767 interval widths with increasing  $N$  happens in a similar<sup>802</sup>  
 768 manner for each  $\Lambda_{\text{NS}}$ , (ii) within  $\sim 10$  observations, me-<sup>803</sup>  
 769 dian measured  $\Lambda_{\text{NS}}$  for all populations lie within 10% of<sup>804</sup>  
 770 the true values, and (iii) it takes approximately 20 events<sup>805</sup>  
 771 to distinguish definitively (with 90% confidence) between<sup>806</sup>  
 772 deformable NSs with  $\Lambda_{\text{NS}} = 2000$  and compact NSs with<sup>807</sup>  
 773  $\Lambda_{\text{NS}} = 500$ , or equivalently to distinguish between hard,<sup>808</sup>  
 774 moderate and soft nuclear equations of state. This is  
 775 comparable to what has been found for binary neutron  
 776 stars [61, 80, 81].

777 So far we have discussed individual realizations of  
 778 NSBH populations. The underlying stochasticity of the

population generation process makes it difficult to draw generalized inferences (from a single realization of an NSBH population) about the measurability of  $\Lambda_{\text{NS}}$ . In order to mitigate this, we discuss ensembles of population draws next. In Fig. 12 we show the measured (median)  $\Lambda_{\text{NS}}$  as a function of the number of observed events, for four population ensembles, with a hundred population draws in each ensemble. Lets focus on the *top left* panel first. In it, we show the measured (median)  $\Lambda_{\text{NS}}$  for all populations in four ensembles, with true  $\Lambda_{\text{NS}} = \{2000, 1500, 1000, 500\}$  from top to bottom. Populations highlighted in color are simply those that we discussed in Fig. 11. Dash-dotted horizontal lines demarcate  $\pm 10\%$  error intervals around the true  $\Lambda_{\text{NS}}$  values. The panel just below it shows the range of  $\Lambda_{\text{NS}}$  that encloses the median measured  $\Lambda_{\text{NS}}$  for 90% of the populations in *each* ensemble. In other words, this panel shows the range of  $\Lambda_{\text{NS}}$  within which the median measured  $\Lambda_{\text{NS}}$  value for 90% of NSBH populations is expected to lie. From these panels, we conclude that our measured  $\Lambda_{\text{NS}}$  values will be within 10% of the *true* value after  $\sim 25$  detections of less deformable neutron stars ( $\Lambda_{\text{NS}} \leq 1000$ ), or after as few as 15 detections of more deformable neutron stars ( $\Lambda_{\text{NS}} \geq 1500$ ). The results discussed in Fig. 10, 11 and the left two panels of Fig. 12 apply to the parameter distribution spanned by the grid G. This distribution allows for  $m_{\text{BH}}$  as low as  $2.7M_{\odot}$  (i.e.  $q = 2$ ). Given that disruptive signatures are strongest for small  $m_{\text{BH}}$ , we now investigate an alternate paradigm <sup>9</sup> with  $m_{\text{BH}} \geq 5M_{\odot}$ ,

<sup>9</sup> We denote our standard paradigm which does not respect the mass-gap as paradigm A; with paradigm B being the scenario where no black hole masses fall within the mass gap  $2 - 5M_{\odot}$ .

consistent with the “mass-gap” suggested by astronomical observations [74–77]. Both right panels of the figure are identical to their corresponding left panels, but drawn under population paradigm B. Under this paradigm, we expectedly find that information accumulation is much slower. It would take  $25 - 40$  detections with  $\rho \geq 10$  under this paradigm, for our (median) measured  $\Lambda_{\text{NS}}$  to converge within 10% of its true value.

Finally, we investigate the statistical uncertainties associated with  $\Lambda_{\text{NS}}$  measurements. We use 90% confidence intervals as our measure of the same. First, we draw an ensemble of a hundred populations each for  $\Lambda_{\text{NS}} = \{500, 1000, 1500, 2000\}$ . For each population  $i$  in each ensemble, we construct its 90% confidence interval  $[\Lambda_{\text{NS},i-}^{90\%}, \Lambda_{\text{NS},i+}^{90\%}]$ . Next, we construct the interval  $[X^-, Y^-]$  that contains  $\Lambda_{\text{NS},i-}^{90\%}$  for 90% of the populations in each ensemble; and similarly  $[X^+, Y^+]$  for  $\Lambda_{\text{NS},i+}^{90\%}$ . Finally, in the left panel of Fig. 13, we show the conservative width  $|Y^+ - X^-|$  that contains the 90% confidence intervals for 90% of all populations in each ensemble<sup>10</sup>. From top to bottom, the population  $\Lambda_{\text{NS}}$  decreases from  $\Lambda_{\text{NS}} = 2000 \rightarrow 500$ , corresponding to decreasingly deformable NSs with softer equations of state. We observe the following: (i) for moderately-hard to hard equations of state with  $\Lambda_{\text{NS}} \geq 1000$ , we can constrain  $\Lambda_{\text{NS}}$  within ±50% using only  $10 - 20$  events, and within ±25% (marked by black circles) with  $25 - 40$  events; (ii) for softer equations of state with  $\Lambda_{\text{NS}} < 1000$ , we will achieve the same accuracy with  $20 - 30$  and  $50+$  events, respectively; and (iii) for the first 5 or so observations, our measurement spans the entire prior allowed range:  $\Lambda_{\text{NS}} \in [0, 4000]$ , as shown by the plateauing of the 90% confidence intervals towards the left edge to 90% of 4000, i.e. 3600. The right panel in Fig. 13 is identical to the left one, with the difference that populations are drawn under paradigm B, which does *not* allow for BH masses to fall within the mass-gap. We find that for NSs with  $\Lambda_{\text{NS}} \leq 1000$ , it would take  $25 - 40$  events to constrain  $\Lambda_{\text{NS}}$  within ±50% and  $50+$  events to constrain it within ±25%. This is somewhat slower than paradigm A, as is to be expected since here we preclude the lowest mass ratios, which correspond to signals with largest tidal signatures. For  $\Lambda_{\text{NS}} > 1000$  we find that we can constrain  $\Lambda_{\text{NS}}$  within ±50% with a similar number of events as for paradigm A, but will need more ( $30 - 40$ , as compared to  $25 - 40$ ) events to further constrain it to within ±25% of the true value. Under either paradigms, we find that measuring  $\Lambda_{\text{NS}}$  better than 25% will require  $\mathcal{O}(10^2)$  observations of disruptive NSBH mergers.

To summarize, in this section we study the improvement in our measurement of NS deformability parameter  $\Lambda_{\text{NS}}$  with an increasing number of events. We do so by simulating plausible populations of disrupting NSBH binaries (with  $\rho \geq 10$ ). We find that: (i) for more de-

formable neutron stars (harder equation of states), the median measured value of  $\Lambda_{\text{NS}}$  comes within 10% of the true value with as few as 10 events, while achieving the same accuracy for softer equations of state will take  $15 - 20$  source detections; (ii) the statistical uncertainty associated with  $\Lambda_{\text{NS}}$  measurement shrinks to within ±50% with  $10 - 20$  events, and to within ±25% with  $50+$  events, when source  $\Lambda_{\text{NS}} \geq 1000$ ; (iii) for softer equations of state, the same could take  $25 - 40$  and  $50+$  events, respectively for the two uncertainty thresholds; and (iv) if BHs really do observe the astrophysical mass-gap, the information accumulation is somewhat slower than if they do not. We conclude that within  $20 - 30$  observations, aLIGO would begin to place very interesting bounds on the NS deformability, which would allow us to rule out or rank different equations of state for neutron star matter. Our key findings are summarized in Fig. 12 and 13.

## VI. DISCUSSION

The pioneering terrestrial observation of gravitational waves by Advanced LIGO harbingers the dawn of an era of gravitational-wave astronomy where observations, more than theory, would play the driving role. Binaries of compact stellar objects evolve under the radiation reaction force of emitting gravitational waves.

Conventional astronomical methods have, to date, made observations of 2500 NSs with masses between  $1.25 - 2.1M_{\odot}$  [63, 82–86], although tightly clustered within  $1.35 \pm 0.5M_{\odot}$  [63]. Observations of over 2500 NSs have shown that the spin of NSs  $|\vec{\chi}_{\text{NS}}|$  have magnitudes that are  $< 1\%$  [64]. On the other hand, indirect observations of stellar-mass BHs place their masses between  $5 - 35M_{\odot}$ , with their spin angular momenta  $|\vec{\chi}_{\text{BH}}|$  ranging from small to nearly extremal (Kerr) values (see, e.g., Refs. [87–89] for examples of nearly extremal estimates of BH spins, Refs. [90, 91] for recent reviews of astrophysical BH spin measurements, and Figure 5 of Ref. [64] for a comparison of NS and BH spins).

We find that non-inclusion of tidal effects leads to systematic biases in the measurement of non-tidal parameters. Consider first the binary chirp mass  $\mathcal{M}_c := M\eta^{3/5}$  where  $M$  is the binary total mass, and  $\eta := m_{\text{BH}}m_{\text{NS}}/M^2$  is the dimensionless mass-ratio. We find that for realistic (moderate) SNRs, i.e.  $\rho \lesssim 30$ , not including tidal effects introduces a barely measurable bias that remains below 50% of the statistical uncertainty of the  $\mathcal{M}_c$  measurement itself. For higher signal strengths, we find that the underlying statistical uncertainty decreases enough for the systematic bias to become comparable to it for  $\rho = 50 - 70$  and higher. This is expected because chirp mass is fairly accurately determined by the inspiral, where tidal effects are weak. Next, we consider the mass-ratio  $\eta$ . We find that only if the NS is quite deformable (with  $\Lambda_{\text{NS}} = 2000$ ), and has a companion BH whose mass is  $m_{\text{BH}} \lesssim 4.5M_{\odot}$  (i.e. in the astrophysical

<sup>10</sup> Drawn under paradigm A.

“mass-gap” [74–77]), will the systematic bias in  $\eta$  measurement become comparable to its statistical uncertainties at SNRs  $\rho \leq 30$ . For SNRs  $\rho \gtrsim 30$ , however, not including tidal effects is very likely to *significantly* bias the mass-ratio estimate for NSBH binaries. Finally, we consider the spin on the black hole  $\chi_{\text{BH}}$ . We find that  $\chi_{\text{BH}}$  measurements are affected in a similar way to  $\eta$ . By not including tidal effects, we compromise our measurement of  $\chi_{\text{BH}}$  significantly only if signal  $\rho \gtrsim 30$ . Overall, we learn an important thing. Bayesian parameter estimation algorithms aimed at identifying NSBH binaries with low latency in order to alert electromagnetic (EM) observers in time to establish a possible coincident observation of a GRB [92–95] can use BBH templates to look for NSBH systems with aLIGO. This is so because the primary requirement of the EM follow-up effort is rapid classification of a binary as an NSBH system, which can be achieved just as easily with BBH templates, purely on the basis of the smaller component’s mass. Another conclusion we draw is that detection searches are unaffected by the choice of ignoring tidal effects in matched-filtering templates.

The choices that determine the population are important here, and were made as follows. Neutron star mass is fixed for signals at  $1.35M_{\odot}$ , and its spin  $\chi_{\text{NS}} = 0$ . Black hole mass is sampled uniformly from the range  $[2, 5] \times 1.35 = [2.7, 6.75]M_{\odot}$ . Our choice here is given by the intersection set of the mass range that allows for neutron star disruption and the range supported by the waveform model LEA+ [45, 53, 96]. Black hole spin is sampled uniformly from the *aligned* range, i.e.  $\chi_{\text{BH}} \in [0, +1]$ . The true deformability is fixed once per population, sampled uniformly from the range  $\Lambda_{\text{NS}} \in [0, 2000]$ . In order to keep the computational cost tractable, we make a further approximation. We inject signals into zero noise at different SNRs and recover their parameters from Bayesian inferencing for a fixed set of binaries, whose parameters lie on a uniform grid given by:  $q = \{2, 3, 4, 5\} \times \chi_{\text{BH}} = \{-0.5, 0, 0.5, 0.75\} \times \Lambda_{\text{NS}} = \{500, 800, 1000, 1500, 2000\} \times \rho = \{10, 20, 30, 50, 70\}$ . Once the population parameters have been selected, each event’s parameters are replaced by their nearest neighbor in the above set. We make sure that this approximation is conservative by keeping our population sampling ranges within the conservative side of the range spanned by the above set. With the caveats laid out, we report our results in Sec. V.

In addition, we probe two paradigms, one that allows for BH masses to lie within the astrophysical mass-gap (paradigm A), and one that does not (paradigm B). For paradigm A, we find the following: (i) for the softer equations of state that result in less deformable neutron stars, 15 – 20 detections are sufficient for our median measured value of  $\Lambda_{\text{NS}}$  to lie within 10% of the true value. (ii) For NSBH populations with more deformable NSs ( $\Lambda_{\text{NS}} \geq 1000$ ), the same is achievable within as few as 10 realistic observations. (iii) The statistical uncertainty associated with  $\Lambda_{\text{NS}}$  measurement can be restricted to be within  $\pm 50\%$  using 10 – 20 obser-

vations when  $\Lambda_{\text{NS}} \geq 1000$ ), and using 25 – 40 observations for softer equations of state. All of the above is possible within a few years of design aLIGO operation [62], if astrophysical BHs do indeed have masses between  $\leq 5M_{\odot}$  (i.e. in the mass-gap). However, further restricting  $\Lambda_{\text{NS}}$  will require 50+ NSBH observations. For paradigm B, we find the information accumulation to be somewhat slower. While the quantitative inferences for  $\Lambda_{\text{NS}} \geq 1000$  populations are not affected significantly, we find  $\mathcal{O}(10 - 20)\%$  more events are required to attain the same measurement accuracy as under paradigm A. We conclude that within as few as 20 – 30 observations of disruptive NSBH mergers, aLIGO will begin to place interesting bounds on NS deformability. This, amongst other things, will allow us to rank different equations of state for neutron star matter from most to least likely, with a few years’ time-scale.

We find that when the BH is sufficiently spinning in the prograde sense, with  $\chi_{\text{BH}} \gtrsim +0.7$ , even at a relatively possible signal strengths ( $\rho = 20$ ), we can begin to constraint  $\Lambda_{\text{NS}}$  at the level of  $\pm 75\%$  errors with a 90% confidence level. If the signal is stronger, say  $\rho = 30$ , we can constraint  $\Lambda_{\text{NS}}$  better with only  $\pm 50\%$  errors, for binaries with large BH spins. This trend continues as we vary the SNR from  $\rho = 30 - 50$  upwards. In other words, with a single but moderately loud NSBH signal observation, Advanced LIGO will begin to put constraints on NS matter properties. These constraints can consequently be used to assess the likelihood of different equations of state for nuclear matter, and possibly narrow the range they span.

Also note that more a recent work that improves upon the waveform model we use in this study has been published [65], but it provides only an amplitude model which needs to be (in future) augmented with a compatible phase model. In addition, accuracy of the underlying numerical simulations used to calibrate the waveform model used here have not been verified against independent codes so far. It is therefore difficult to assess the combined modeling error and its effect on our results. They are, therefore, limited by the limitations of our waveform model. However, we expect the combined effect of modeling errors to not change our qualitative conclusions.

## ACKNOWLEDGMENTS

We thank Ben Lackey, Francesco Pannarale, Francois Foucart, and Duncan Brown for helpful discussions. We gratefully acknowledge support for this research at CITA from NSERC of Canada, the Ontario Early Researcher Awards Program, the Canada Research Chairs Program, and the Canadian Institute for Advanced Research; at Caltech from the Sherman Fairchild Foundation and NSF grants PHY-1404569 and AST-1333520; at Cornell from the Sherman Fairchild Foundation and NSF grants PHY-1306125 and AST-1333129; and at Princeton from NSF

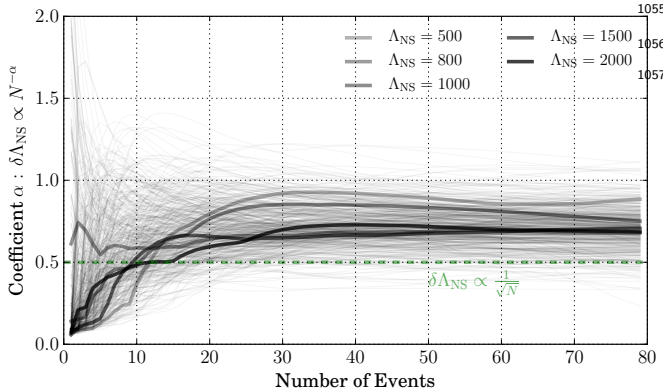


FIG. 14. Assuming a power-law dependence of the measurement error on the number of events:  $\delta\Lambda_{NS} \propto 1/N^\alpha$ , we show  $\alpha$  in this figure as a function of the number of observed events  $N$ . Shown are five families of 100 population draws each, with each family corresponding to one of  $\Lambda_{NS} = \{500, 800, 1000, 1500, 2000\}$ . Each grey curve corresponds to one of these  $100 \times 5 = 500$  populations. The thicker curves, one from each family, shows the population we discussed in Fig. 10–11. We find that a power-law is a good approximation for the concerned dependence, and information accumulates *faster* than  $1/\sqrt{N}$ . We estimate  $\alpha \simeq 0.7^{+0.2}_{-0.2}$ .

Fisher-matrix studies [53], and as for  $N$ , we assume the form  $\delta\Lambda_{NS} \propto \Lambda_{NS}^\beta$ . From each set of 100 populations with a given  $\Lambda_{NS}$  value, we draw one at random, and

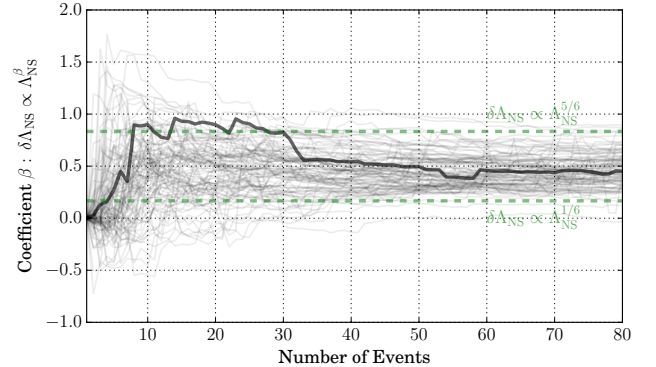


FIG. 15. In this figure, which is similar to Fig. 14, we quantify the dependence of  $\delta\Lambda_{NS}$  on  $\Lambda_{NS}$  itself. Of the five families of simulated NSBH populations, we construct 100 independent sets taking one population from each family. With each of these 100 sets, and assuming a power-law dependence:  $\delta\Lambda_{NS} \propto \Lambda_{NS}^\beta$ , we estimate  $\beta$  and show it in this figure as a function of the number of observed events  $N$ . The thicker curve corresponds to the populations discussed in Fig. 11. We find that  $\beta$  can be estimated to lie within  $[1/6, 5/6]$  with a likely value close to  $1/2$ . Since  $0 < \beta < 1$ , the relative error  $\delta\Lambda_{NS}/\Lambda_{NS}$  decreases as the star gets more deformable, while the absolute error  $\delta\Lambda_{NS}$  increases.

grant PHY-1305682 and the Simons Foundation. Calculations were performed at the Vulcan supercomputer at the Albert Einstein Institute; H.P. and P.K. thank the Albert-Einstein Institute, Potsdam, for hospitality during part of the time where this research was completed.

form a set of 5 similarly drawn populations, one for each of  $\Lambda_{NS} = \{500, 800, 1000, 1500, 2000\}$ . With each set, we determine  $\beta$  for different number of observed events  $N$ . In all, we make 100 independent 5-population sets and show the value of  $\beta$  measured from each in Fig. 15. We find that the assumed relation  $\delta\Lambda_{NS} \propto \Lambda_{NS}^\beta$  gets fairly robust for larger values of  $N$ , with  $\beta$  converging to  $\beta = 0.5^{+0.33}_{-0.33}$ . The fact that  $0 < \beta < 1$  implies that the relative error  $\delta\Lambda_{NS}/\Lambda_{NS}$  decreases with increasing  $\Lambda_{NS}$ , while the absolute error increases. From these results, we conclude that the measurement uncertainty for  $\Lambda_{NS}$  after  $N$  observations is

$$\delta\Lambda_{NS} \propto \frac{\Lambda_{NS}^{0.5^{+0.33}_{-0.33}}}{N^{0.7^{+0.2}_{-0.2}}} \quad (\text{A1})$$

We also find that while these results are inferred from paradigm A populations, paradigm B gives very similar results.

## REFERENCES

- [1] D. Shoemaker (LIGO Collaboration), “Advanced LIGO anticipated sensitivity curves,” (2010), LIGO Document T0900288-v3.
- [2] B. P. Abbott *et al.* (LIGO Scientific Collaboration, Virgo Collaboration), *Phys. Rev. Lett.* **116**, 061102 (2016), arXiv:1602.03837 [gr-qc].
- [3] The Virgo Collaboration, “Advanced Virgo Baseline sign,” (2009), [VIR-0027A-09].
- [4] F. Acernese *et al.* (Virgo Collaboration), *Class. Quantum Grav.* **32**, 024001 (2015), arXiv:1408.3978 [gr-qc].
- [5] Y. Aso, Y. Michimura, K. Somiya, M. Ando, O. Miyakawa, T. Sekiguchi, D. Tatsumi, and H. Yamaamoto (The KAGRA Collaboration), *Phys. Rev. D* **88**, 043007 (2013), arXiv:1306.6747 [gr-qc].
- [6] K. Somiya (KAGRA Collaboration), *Class. Quantum Grav.* **29**, 124007 (2012), arXiv:1111.7185 [gr-qc].
- [7] C. S. Unnikrishnan, *International Journal of Modern Physics D* **22**, 1341010 (2013).
- [8] F. X. Timmes, S. E. Woosley, and T. A. Weaver, *Astrophys. J.* **457**, 834 (1996), arXiv:astro-ph/9510136 [astro-ph].
- [9] C. L. Fryer, *Astrophys. J.* **522**, 413 (1999), arXiv:astro-ph/9902315 [astro-ph].
- [10] S. E. Woosley, A. Heger, and T. A. Weaver, *Rev. Mod. Phys.* **74**, 1015 (2002).
- [11] K. Belczynski, T. Bulik, C. L. Fryer, A. Ruiter, F. Valsechi, J. S. Vink, and J. R. Hurley, *apj* **714**, 1217 (2010), arXiv:0904.2784 [astro-ph.SR].
- [12] K. Belczynski, M. Dominik, T. Bulik, R. O’Shaughnessy, C. Fryer, and D. E. Holz, *Astrophys. J. Lett.* **715**, L138 (2010), arXiv:1004.0386 [astro-ph.HE].
- [13] M. Dominik, E. Berti, R. O’Shaughnessy, I. Mandel, K. Belczynski, C. Fryer, D. Holz, T. Bulik, and F. Panarale, *Astrophys. J.* **806**, 263 (2015), arXiv:1405.7016 [astro-ph.HE].
- [14] K. Belczynski, V. Kalogera, F. A. Rasio, R. E. Taam, and T. Bulik, *Astrophys. J.* **662**, 504 (2007), arXiv:astro-ph/0612032 [astro-ph].
- [15] C. L. Fryer, K. Belczynski, G. Wiktorowicz, M. Dominik, V. Kalogera, and D. E. Holz, *apj* **749**, 91 (2012), arXiv:1110.1726 [astro-ph.SR].
- [16] N. Wex and S. Kopeikin, *Astrophys. J.* **514**, 388 (1999), arXiv:astro-ph/9811052 [astro-ph].
- [17] R. Narayan, T. Piran, and A. Shemi, *Astrophys. J.* **379**, L17 (1991).
- [18] I. Mandel, C.-J. Haster, M. Dominik, and K. Belczynski, (2015), 10.1093/mnrasl/slv054, arXiv:1503.03172 [astro-ph.HE].
- [19] B. P. Abbott *et al.* (Virgo, LIGO Scientific), (2016), arXiv:1602.03842 [astro-ph.HE].
- [20] D. Psaltis, M. van der Klis, T. Strohmayer, L. Bildsten, J. McClintock, R. Remillard, P. Charles, M. Coe, J. Heise, J. in ’t Zand, V. Kaspi, M. Roberts, A. Harding, F. Verbunt, W. Lewin, R. Fender, E. Kuulkers, A. Norrington, A. Schwope, B. Warner, P. Kahabka, E. van den Heuvel, G. Fabbiano, N. White, A. King, P. Woods, C. Thompson, K. Hurley, R. Sari, S. Djorgovski, and T. Tauris, in *Compact Stellar X-ray Sources*, edited by M. v. d. K. Walter Lewin (Cambridge University Press) (2010) p. 708.
- [21] R. A. Remillard and J. E. McClintock, *Ann. Rev. Astron. Astrophys.* **44**, 49 (2006), arXiv:astro-ph/0606352 [astro-ph].
- [22] T. Fragos, M. Tremmel, E. Rantsiou, and K. Belczynski, (2010), arXiv:1001.1107 [astro-ph.HE].
- [23] R. N. Manchester, G. B. Hobbs, A. Teoh, and M. Hobbs, *Astron. J.* **129**, 1993 (2005), arXiv:astro-ph/0412641 [astro-ph].
- [24] J. M. Lattimer, *Ann.Rev.Nucl.Part.Sci.* **62**, 485 (2012), arXiv:1305.3510 [nucl-th].
- [25] B. Margon, M. Lampton, S. Bowyer, and R. Cruddace, *Astrophys. J. Lett.* **169**, L23 (1971).
- [26] H. E. Bond, R. L. White, R. H. Becker, and M. S. O’Brien, *Publ. Astron. Soc. Pac.* **114**, 1359 (2002), arXiv:astro-ph/0208383 [astro-ph].
- [27] R. A. Hulse and J. H. Taylor, *Astrophys. J.* **195**, L51 (1975).
- [28] J. H. Taylor and J. M. Weisberg, *Astrophys. J.* **253**, 908 (1982).
- [29] J. Weisberg, D. Nice, and J. Taylor, *Astrophys.J.* **722**, 1030 (2010), arXiv:1011.0718 [astro-ph.GA].
- [30] H.-T. Janka, T. Eberl, M. Ruffert, and C. L. Fryer, *Astrophys. J.* **527**, L39 (1999), astro-ph/9908290.
- [31] C. L. Fryer, F. G. Oliveira, J. A. Rueda, and R. Ruffini, *Phys. Rev. Lett.* **115**, 231102 (2015), arXiv:1505.02809 [astro-ph.HE].
- [32] J. Abadie, B. P. Abbott, R. Abbott, M. Abernathy, T. Accadia, F. Acernese, C. Adams, R. Adhikari, P. Ajith, B. Allen, and et al. (LIGO Scientific Collaboration, Virgo Collaboration), *Class. Quantum Grav.* **27**, 173001 (2010), arXiv:1003.2480 [astro-ph.HE].
- [33] D. Eichler, M. Livio, T. Piran, and D. N. Schramm, *Nature* **340**, 126 (1989).
- [34] R. Narayan, B. Paczynski, and T. Piran, *Astrophys. J. Lett.* **395**, L83 (1992), astro-ph/9204001.
- [35] R. Mochkovitch, M. Hernanz, J. Isern, and X. Martin, *Nature* **361**, 236 (1993).
- [36] S. D. Barthelmy *et al.*, *Nature* **438**, 994 (2005), arXiv:astro-ph/0511579 [astro-ph].
- [37] D. B. Fox, D. A. Frail, P. A. Price, S. R. Kulkarni, E. Berger, T. Piran, A. M. Soderberg, S. B. Cenko, P. B. Cameron, A. Gal-Yam, M. M. Kasliwal, D.-S. Moon, F. A. Harrison, E. Nakar, B. P. Schmidt, B. Penprase, R. A. Chevalier, P. Kumar, K. Roth, D. Watson, B. L. Lee, S. Shectman, M. M. Phillips, M. Roth, P. J. McCarthy, M. Rauch, L. Cowie, B. A. Peterson, J. Rich, N. Kawai, K. Aoki, G. Kosugi, T. Totani, H.-S. Park, A. MacFadyen, and K. C. Hurley, *Nature* **437**, 845 (2005), astro-ph/0510110.
- [38] N. Gehrels, C. L. Sarazin, P. T. O’Brien, B. Zhang, L. Barbier, S. D. Barthelmy, A. Blustin, D. N. Burrows, J. Cannizzo, J. R. Cummings, M. Goad, S. T. Holland, C. P. Hurkett, J. A. Kennea, A. Levan, C. B. Markwardt, K. O. Mason, P. Meszaros, M. Page, D. M. Palmer, E. Rol, T. Sakamoto, R. Willingale, L. Angelini, A. Beardmore, P. T. Boyd, A. Breeveld, S. Campana, M. M. Chester, G. Chincarini, L. R. Cominsky, G. Cusumano, M. de Pasquale, E. E. Fenimore, P. Giommi, C. Gronwall, D. Grupe, J. E. Hill, D. Hinshaw, J. Hjorth, D. Hullinger, K. C. Hurley, S. Klose, S. Kobayashi, C. Kouveliotou, H. A. Krimm, V. Mangano, F. E. Marshall, K. McGowan, A. Moretti,

- R. F. Mushotzky, K. Nakazawa, J. P. Norris, J. A<sub>1259</sub>  
 1196 Nousek, J. P. Osborne, K. Page, A. M. Parsons, S. Pa<sub>1260</sub>  
 1197 tel, M. Perri, T. Poole, P. Romano, P. W. A. Roming,<sub>1261</sub>  
 1198 S. Rosen, G. Sato, P. Schady, A. P. Smale, J. Sollerman,<sub>1262</sub>  
 1200 R. Starling, M. Still, M. Suzuki, G. Tagliaferri, T. Taka<sub>1263</sub>  
 1201 hashi, M. Tashiro, J. Tueller, A. A. Wells, N. E. White,<sub>1264</sub>  
 1202 and R. A. M. J. Wijers, *Nature* **437**, 851 (2005), astro<sub>1265</sub>  
 1203 ph/0505630.<sub>1266</sub>
- [39] M. Shibata, M. D. Duez, Y. T. Liu, S. L. Shapiro, and B. C. Stephens, *Phys. Rev. Lett.* **96**, 031102 (2006), arXiv:astro-ph/0511142 [astro-ph].
- [40] V. Paschalidis, M. Ruiz, and S. L. Shapiro, *Astrophys. J.* **806**, L14 (2015), arXiv:1410.7392 [astro-ph.HE].
- [41] N. R. Tanvir, A. J. Levan, A. S. Fruchter, J. Hjorth, R. A. Hounsell, K. Wiersema, and R. L. Tunnicliffe, *Nature* **500**, 547 (2013), arXiv:1306.4971 [astro-ph.HE].
- [42] F. Foucart, E. O'Connor, L. Roberts, M. D. Duez, R. Haas, L. E. Kidder, C. D. Ott, H. P. Pfeiffer, M. A. Scheel, and B. Szilagyi, *Phys. Rev. D* **91**, 124021 (2015), arXiv:1502.04146 [astro-ph.HE].
- [43] G. Lovelace, M. D. Duez, F. Foucart, L. E. Kidder, H. P. Pfeiffer, M. A. Scheel, and B. Szilagyi, *Class. Quant. Grav.* **30**, 135004 (2013), arXiv:1302.6297 [gr-qc].
- [44] M. B. Deaton, M. D. Duez, F. Foucart, E. O'Connor, C. D. Ott, L. E. Kidder, C. D. Muhlberger, M. A. Scheel, and B. Szilagyi, *Astrophys. J.* **776**, 47 (2013), arXiv:1304.3384 [astro-ph.HE].
- [45] F. Foucart, *Phys. Rev. D* **86**, 124007 (2012), arXiv:1207.6304 [astro-ph.HE].
- [46] F. Foucart, L. Buchman, M. D. Duez, M. Grudich, L. E. Kidder, I. MacDonald, A. Mroue, H. P. Pfeiffer, M. A. Scheel, and B. Szilagyi, *Phys. Rev. D* **88**, 064017 (2013), arXiv:1307.7685 [gr-qc].
- [47] M. Shibata and K. Taniguchi, *Phys. Rev. D* **77**, 084015 (2008), arXiv:0711.1410 [gr-qc].
- [48] V. Ferrari, L. Gualtieri, and F. Pannarale, *Phys. Rev. D* **81**, 064026 (2010), arXiv:0912.3692 [gr-qc].
- [49] K. Kawaguchi, K. Kyutoku, H. Nakano, H. Okawa, M. Shibata, and K. Taniguchi, *Phys. Rev. D* **92**, 024014 (2015), arXiv:1506.05473 [astro-ph.HE].
- [50] B. P. Abbott *et al.* (LIGO Scientific Collaboration, Virgo Collaboration), *Living Rev. Rel.* **19** (2016), 10.1007/lrr-2016-1, arXiv:1304.0670v3 [gr-qc].
- [51] É. É. Flanagan and T. Hinderer, *Phys. Rev. D* **77**, 021502 (2008), arXiv:0709.1915.
- [52] K. Kyutoku, M. Shibata, and K. Taniguchi, *Phys. Rev. D* **82**, 044049 (2010), arXiv:1008.1460 [astro-ph.HE].
- [53] B. D. Lackey, K. Kyutoku, M. Shibata, P. R. Brady, and J. L. Friedman, *Phys. Rev. D* **89**, 043009 (2014), arXiv:1303.6298 [gr-qc].
- [54] F. Pannarale, E. Berti, K. Kyutoku, B. D. Lackey, and M. Shibata, (2015), arXiv:1509.06209 [gr-qc].
- [55] J. Vines, É. É. Flanagan, and T. Hinderer, *Phys. Rev. D* **83**, 084051 (2011), arXiv:1101.1673 [gr-qc].
- [56] A. Maselli, L. Gualtieri, and V. Ferrari, *Phys. Rev. D* **88**, 104040 (2013), arXiv:1310.5381 [gr-qc].
- [57] K. Barkett, M. A. Scheel, R. Haas, C. D. Ott, S. Bernuzzi, D. A. Brown, B. Szilagyi, J. D. Kaplan, J. Lippuner, C. D. Muhlberger, F. Foucart, and M. D. Duez, *Phys. Rev. D* **93**, 044064 (2016), arXiv:1509.05782 [gr-qc].
- [58] K. Yagi and N. Yunes, *Phys. Rev. D* **89**, 021303 (2014), arXiv:1310.8358 [gr-qc].
- [59] B. D. Lackey, K. Kyutoku, M. Shibata, P. R. Brady, and J. L. Friedman, *Phys. Rev. D* **85**, 044061 (2012), arXiv:1109.3402 [astro-ph.HE].
- [60] M. Vallisneri, *Phys. Rev. D* **77**, 042001 (2008), arXiv:gr-qc/0703086 [GR-QC].
- [61] W. Del Pozzo, T. G. F. Li, M. Agathos, C. Van Den Broeck, and S. Vitale, *Phys. Rev. Lett.* **111**, 071101 (2013), arXiv:1307.8338 [gr-qc].
- [62] J. Abadie *et al.* (LIGO Scientific Collaboration), *Class. Quantum Grav.* **27**, 173001 (2010), arXiv:1003.2480 [gr-qc].
- [63] “stellarcollapse.org – Neutron star mass tables,” <http://www.stellarcollapse.org/nsmasses>.
- [64] M. C. Miller and J. M. Miller, *Phys. Rept.* **548**, 1 (2014), arXiv:1408.4145 [astro-ph.HE].
- [65] F. Pannarale, E. Berti, K. Kyutoku, B. D. Lackey, and M. Shibata, *Phys. Rev. D* **92**, 084050 (2015), arXiv:1509.00512 [gr-qc].
- [66] A. Taracchini, Y. Pan, A. Buonanno, E. Barausse, M. Boyle, T. Chu, G. Lovelace, H. P. Pfeiffer, and M. A. Scheel, *Phys. Rev. D* **86**, 024011 (2012), arXiv:1202.0790 [gr-qc].
- [67] A. Buonanno and T. Damour, *Phys. Rev. D* **59**, 084006 (1999), arXiv:gr-qc/9811091 [gr-qc].
- [68] A. Taracchini, A. Buonanno, Y. Pan, T. Hinderer, M. Boyle, D. A. Hemberger, L. E. Kidder, G. Lovelace, A. H. Mroue, H. P. Pfeiffer, M. A. Scheel, B. Szilagyi, N. W. Taylor, and A. Zenginoglu, *Phys. Rev. D* **89** (R), 061502 (2014), arXiv:1311.2544 [gr-qc].
- [69] M. Prrer, (2015), arXiv:1512.02248 [gr-qc].
- [70] P. Kumar, K. Barkett, S. Bhagwat, N. Afshari, D. A. Brown, G. Lovelace, M. A. Scheel, and B. Szilgyi, *Phys. Rev. D* **92**, 102001 (2015), arXiv:1507.00103 [gr-qc].
- [71] P. Kumar, T. Chu, H. Fong, H. P. Pfeiffer, M. Boyle, D. A. Hemberger, L. E. Kidder, M. A. Scheel, and B. Szilagyi, (2016), arXiv:1601.05396 [gr-qc].
- [72] D. Foreman-Mackey, D. W. Hogg, D. Lang, and J. Goodman, arXiv 125, 306 (2013), arXiv:1202.3665 [astro-ph.IM].
- [73] M. Prrer, M. Hannam, and F. Ohme, (2015), arXiv:1512.04955 [gr-qc].
- [74] C. D. Bailyn, R. K. Jain, P. Coppi, and J. A. Orosz, *Astrophys. J.* **499**, 367 (1998), arXiv:astro-ph/9708032 [astro-ph].
- [75] V. Kalogera and G. Baym, *Astrophys. J.* **470**, L61 (1996), arXiv:astro-ph/9608059 [astro-ph].
- [76] L. Kreidberg, C. D. Bailyn, W. M. Farr, and V. Kalogera, *Astrophys.J.* **757**, 36 (2012), arXiv:1205.1805 [astro-ph.HE].
- [77] T. B. Littenberg, B. Farr, S. Coughlin, V. Kalogera, and D. E. Holz, (2015), arXiv:1503.03179 [astro-ph.HE].
- [78] B. Kiziltan, A. Kottas, M. De Yoreo, and S. E. Thorsett, *Astrophys. J.* **778**, 66 (2013).
- [79] C. Markakis, J. S. Read, M. Shibata, K. Uryu, J. D. E. Creighton, and J. L. Friedman, in *On recent developments in theoretical and experimental general relativity, astrophysics and relativistic field theories. Proceedings, 12th Marcel Grossmann Meeting on General Relativity, Paris, France, July 12-18, 2009. Vol. 1-3* (2010) pp. 743–745, arXiv:1008.1822 [gr-qc].
- [80] K. Chatzioannou, K. Yagi, A. Klein, N. Cornish, and N. Yunes, *Phys. Rev. D* **92**, 104008 (2015), arXiv:1508.02062 [gr-qc].
- [81] M. Agathos, J. Meidan, W. D. Pozzo, T. G. F. Li, M. Tompitak, J. Veitch, S. Vitale, and C. V. D. Broeck,

- 1323 Phys. Rev. D **92**, 023012 (2015), arXiv:1503.05405 [gr-<sup>1346</sup>  
1324 qc].<sup>1347</sup>
- [82] A. Lyne, M. Burgay, M. Kramer, A. Possenti, R. Manchester,<sup>1348</sup>  
esther, *et al.*, Science **303**, 1153 (2004), arXiv:astro-<sup>1349</sup>  
ph/0401086 [astro-ph].<sup>1350</sup>
- [83] P. Demorest, T. Pennucci, S. Ransom, M. Roberts, and<sup>1351</sup>  
J. Hessels, Nature **467**, 1081 (2010), arXiv:1010.5788<sup>1352</sup>  
[astro-ph.HE].<sup>1353</sup>
- [84] J. Antoniadis, P. C. C. Freire, N. Wex, T. M. Tauris, R. S.<sup>1354</sup>  
Lynch, M. H. van Kerkwijk, M. Kramer, C. Bassa, V. S.<sup>1355</sup>  
Dhillon, T. Driebe, J. W. T. Hessels, V. M. Kaspi, V. I.<sup>1356</sup>  
Kondratiev, N. Langer, T. R. Marsh, M. A. McLaughlin,<sup>1357</sup>  
T. T. Pennucci, S. M. Ransom, I. H. Stairs, J. van Leeuwen,<sup>1358</sup>  
J. P. W. Verbist, and D. G. Whelan, Science **340**, 448  
(2013), arXiv:1304.6875 [astro-ph.HE].<sup>1359</sup>
- [85] “Australia Telescope National Facility – catalog,” <http://www.atnf.csiro.au/research/pulsar/psrcat/>.<sup>1360</sup>
- [86] “McGill Online Magnetar Catalog,” <http://www.physics.mcgill.ca/~pulsar/magnetar/main.html>.<sup>1361</sup>
- [87] J. E. McClintock, R. Shafee, R. Narayan, R. A. Remillard,<sup>1362</sup>  
S. W. Davis, and L.-X. Li, Astrophys. J. **652**, 518<sup>1363</sup>  
(2006).<sup>1364</sup>
- [88] J. Miller, C. Reynolds, A. Fabian, G. Miniutti, and<sup>1365</sup>  
L. Gallo, Astrophys.J. **697**, 900 (2009), arXiv:0902.2840  
[astro-ph.HE].
- [89] L. Gou, J. E. McClintock, R. A. Remillard, J. F. Steiner,  
M. J. Reid, *et al.*, Astrophys.J. **790**, 29 (2014).
- [90] J. E. McClintock, R. Narayan, and J. F. Steiner, Space Sci.Rev. **183**, 295 (2014), arXiv:1303.1583 [astro-ph.HE].
- [91] C. S. Reynolds, Space Science Reviews **183**, 277 (2014),  
arXiv:1302.3260 [astro-ph.HE].
- [92] J. Abadie, B. P. Abbott, R. Abbott, T. D. Abbott,  
M. Abernathy, T. Accadia, F. Acernese, C. Adams,  
R. Adhikari, C. Affeldt, and et al., Astron. Astrophys.  
**541**, A155 (2012), arXiv:1112.6005.
- [93] L. P. Singer *et al.*, Astrophys. J. **795**, 105 (2014),  
arXiv:1404.5623 [astro-ph.HE].
- [94] L. P. Singer and L. R. Price, Phys. Rev. **D93**, 024013  
(2016), arXiv:1508.03634 [gr-qc].
- [95] C. Pankow, P. Brady, E. Ochsner, and  
R. O’Shaughnessy, Phys. Rev. **D92**, 023002 (2015),  
arXiv:1502.04370 [gr-qc].
- [96] F. Foucart, M. B. Deaton, M. D. Duez, L. E. Kidder,  
I. MacDonald, C. D. Ott, H. P. Pfeiffer, M. A. Scheel,  
B. Szilagyi, and S. A. Teukolsky, Phys. Rev. D **87**,  
084006 (2013), arXiv:1212.4810 [gr-qc].